Structured and disordered regions of Ataxin-2 contribute differently to the specificity and efficiency of mRNP granule formation.

Arnas Petrauskas[1*], Daniel L. Fortunati[1*], Amanjot Singh[2], Arvind Reddy Kandi[5], Sai Shruti Pothapragada[2], Khushboo Agrawal[3,4], Joern Huelsmeier[1], Jens Hillebrand[1], Georgia Brown[1], Dhananjay Chaturvedi[2], Jongbo Lee[6], Chunghun Lim[6], Georg Auburger[7], K. VijayRaghavan[2], Mani Ramaswami[1,2†] and Baskar Bakthavachalu[3,5†].

[1]Trinity College Institute of Neuroscience, School of Genetics and Microbiology, Smurfit Institute of Genetics and School of Natural Sciences, Trinity College Dublin, Dublin-2 Ireland. [2]National Centre for Biological Sciences, TIFR, Bangalore 560065, India. [3]Tata Institute for Genetics and Society Centre at inStem, Bellary Road, Bangalore 560065, India. [4]School of Biotechnology, Amrita Vishwa Vidyapeetham University, Kollam-690525, Kerala, India. [5]School of Basic Sciences, Indian Institute of Technology, Mandi 175005, India. [6]Department of Biological Sciences, Ulsan National Institute of Science and Technology (UNIST), 50 UNIST-gil, Ulsan 44919, Republic of Korea. [7]Experimental Neurology, Medical School, Goethe University, 60590, Frankfurt, Germany.

*These authors contributed equally to this work.

† **Correspondence**:
mani.ramaswami@tcd.ie; Phone +353 (1) 896 8400
baskar@iitmandi.ac.in; Phone +91-1905-267705

Running Title: Ataxin-2 PAM2:PABP interactions specify granule composition

Keywords: Ataxin-2, TRIBE, mRNA, PABP, Disordered Regions, Subcellular Organization, Stress Granule, Neurodegeneration, RNP Granule, *Drosophila*.

ABSTRACT:

Ataxin-2 (*ATXN2*) is a gene implicated in spinocerebellar ataxia type II (SCA2), amyotrophic lateral sclerosis (ALS) and Parkinsonism. The encoded protein is a therapeutic target for ALS and related conditions. ATXN2 (or Atx2 in insects) can function in translational activation, translational repression, mRNA stability and in the assembly of mRNP-granules, a process mediated by intrinsically disordered regions (IDRs). Previous work has shown that the LSm (Like-Sm) domain of Atx2, which can help stimulate mRNA translation, antagonizes mRNP-granule assembly. Here we advance these findings through a series of experiments on *Drosophila* and human Ataxin-2 proteins. Results of Targets of RNA-Binding Proteins Identified by Editing (TRIBE), co-localization and immunoprecipitation experiments indicate that a polyA-binding protein (PABP) interacting, PAM2 motif of Ataxin-2 may be a major determinant of the mRNA and protein content of Ataxin-2 mRNP granules. Transgenic experiments in *Drosophila* indicate that while the Atx2-LSm domain may protect against neurodegeneration, structured PAM2- and unstructured IDR-interactions both support Atx2-induced cytotoxicity. Taken together, the data lead to a proposal for how Ataxin-2 interactions are remodelled during translational control and how structured and non-structured interactions contribute differently to the specificity and efficiency of RNP granule condensation as well as to neurodegeneration.

INTRODUCTION:

mRNP granules are intriguing, dynamic membrane-less organelles containing translationally repressed mRNAs, RNA-binding proteins (RBPs), molecular chaperones and a variety of other cellular proteins (Buchan, 2014; Formicola *et al*, 2019; Kiebler & Bassell, 2006; Knowles *et al*, 1996; Martin & Ephrussi, 2009). The formation and composition of mRNP assemblies are determined by base-pairing interactions between mRNAs, protein-protein interactions and RBP-RNA interactions, whose respective contributions may vary across granule types and physiological states (Bevilacqua *et al*, 2022; Matheny *et al*, 2021; Van Treeck & Parker, 2018; Van Treeck *et al*, 2018). Stress granules (SGs) are particularly well-studied granules that form when cellular stress signals mediated by eIF2α kinase activation (Kedersha *et al*, 1999) cause individual mRNPs to arrest in translation and condense into multi-mRNP assemblies (Ivanov *et al*, 2019; Kedersha & Anderson, 2007; Youn *et al*, 2019). Mutations in mRNP granule proteins, including TDP-43, FUS, Ataxin-2, hnRNPA1, hnRNPA2B1, EWSR1, have been associated with ALS and/or other forms of neurodegenerative disease (Cirulli *et al*, 2015; Couthouis *et al*, 2012; Elden *et al*, 2010; Ginsberg *et al*, 1998; Kim *et al*, 2013; Liu *et al*, 2017; Taylor *et al*, 2016; Wolozin & Ivanov, 2019). For this reason, and because TDP-43 and other stress-granule protein aggregates are components of protein inclusions found in ALS and Frontotemporal dementia (FTD), the regulation and cellular functions of stress granules have been topics of considerable fundamental and clinical interest (Cao *et al*, 2020; Li *et al*, 2013; Mallucci *et al*, 2020; Protter & Parker, 2016; Wang *et al*, 2020; Wheeler *et al*, 2016; Wolozin & Ivanov, 2019).

The cast of intermolecular interactions required for mRNP-granule assembly and the precise sequence with which they occur are not yet elucidated (Khong & Parker, 2020; Van Treeck & Parker, 2018). However, many studies show that intrinsically disordered regions (IDRs) found on mRNP-granule proteins contribute substantially to RNP granule assembly (Andrusiak *et al*, 2019; Ash *et al*, 2021; Calabretta & Richard, 2015; Decker *et al*, 2007; Gilks *et al*, 2004; Järvelin *et al*, 2016; Kim *et al*, 2021; Yang *et al*, 2020). In biochemical experiments, such IDRs show the ability to phase separate into liquid-like assemblies (Babinchak & Surewicz, 2020; Han *et al*, 2012; Hyman *et al*, 2014; Kato *et al*, 2012; Lin *et al*, 2017; Murray *et al*, 2017; Murthy *et al*, 2019; Shin & Brangwynne, 2017; Strome & Wood, 1982; Toretsky & Wright, 2014; Yang *et al.*, 2020) The accessibility or activities of IDRs can be tightly regulated by posttranslational modifications, allowing rapid physiological and spatial control over granule

assembly and disassembly (Ash *et al.*, 2021; Bah & Forman-Kay, 2016; Bah *et al*, 2015; Berlow *et al*, 2015; Hofweber & Dormann, 2019; Kwon *et al*, 2013; Rayman *et al*, 2018; Saito *et al*, 2019; Yang *et al.*, 2020).

An important observation is that most IDRs also have the ability to transition from liquid-like states into solid, beta-sheet rich, amyloid-fibrils *in vitro*, particularly at high concentrations achieved in the liquid-phase (Alberti *et al*, 2019; Li *et al.*, 2013; Murray *et al.*, 2017; Patel *et al*, 2015; Ramaswami *et al*, 2013). This, and studies showing that inhibitors of eIF2α kinase or downstream events including SG formation can be protective in animal models of neurodegenerative disease (Chou *et al*, 2017; Halliday *et al*, 2017; Sidrauski *et al*, 2015; Wong *et al*, 2018; Zyryanova *et al*, 2021) have led to a conceptual framework in which: (a) mRNP granules provide a microenvironment where pathogenic protein seeds can form and grow (Bakthavachalu *et al*, 2018; Mandrioli *et al*, 2020; Patel *et al.*, 2015); (b) increased misfolded-protein loads result in inclusion formation, chronic stress signalling and reduced protein translation (Hetz *et al*, 2020; Preissler & Ron, 2019); (c) increased demand on protein handling systems results in multiple cellular defects, notably in the functions of membrane-less organelles (Alberti *et al*, 2017; Azkanaz *et al*, 2019; Jiang *et al*, 2020; Latonen, 2019; Schuller *et al*, 2021). In particular, aberrant SG formation also results in nuclear transport defects which may contribute to cell death and toxicity (Hochberg-Laufer *et al*, 2019; Zhang *et al*, 2018).

Particularly strong support for the role of RNP granule formation in promoting disease comes from studies of Ataxin-2. Loss of Ataxin-2 is cytoprotective in yeast TDP-43 and *Drosophila* TDP-43 or C9ORF72 or Tau models of cytotoxicity (Bakthavachalu *et al.*, 2018; Becker *et al*, 2017; Elden *et al.*, 2010; Huelsmeier *et al*, 2021; Kim *et al*, 2014; Lee *et al*, 2016; Shulman & Feany, 2003). In mouse models for SCA2 or ALS, either genetic loss of *ATXN2* or delivery of antisense oligonucleotides (ASOs) targeting *ATXN2* in the central nervous system, reduced aggregation of TDP-43, increased animal survival and improved motor function (Becker *et al.*, 2017; Scoles *et al*, 2017). These observations have led to ASOs against human *ATXN2* being developed and approved for clinical trials (Biogen, 2021).

Given Ataxin-2's therapeutic significance and multiple roles in biology, it is particularly important to determine which molecular activities of the protein are relevant to disease and to its various biological functions (Kim *et al*, 2020). Across species, Ataxin-2 has three conserved regions: a Like-Sm (LSm) domain, an LSm-associated domain (LSm-AD) and a PAM2 motif,

which is flanked by extended intrinsically disordered regions (IDRs) (Boeynaems *et al*, 2021). Detailed work in *Drosophila* has shown that a c-terminal IDR of Atx2 is selectively required for mRNP assembly into granules (Bakthavachalu *et al.*, 2018). Parallel experiments showing that the IDR is also required for cytotoxicity in *Drosophila* FUS, C9ORF72 and Huntington's disease models suggest RNP-granule formation to be a significant mechanism by which Atx2 promotes neurodegeneration (Bakthavachalu *et al.*, 2018; Huelsmeier *et al.*, 2021). A recent discovery that the Atx2-LSm domain antagonizes IDR-function has led to a model in which the Atx2 cIDR: (a) does not support mRNP assembly when Atx2 is associated with actively translating mRNAs through Atx2-LSm domain interactions; (b) becomes accessible and active in mediating mRNP assembly when LSm-domain interactions break and mRNA translation stalls (Boeynaems *et al.*, 2021; Singh *et al*, 2021).

We now present a series of experiments further elaborating mechanisms by Ataxin-2 functions in mRNA translation and mRNP assembly. These show that the PAM2 motif of Ataxin-2 and its interactions with PABP are not essential for granule assembly but are required to efficiently recruit Atx2-target mRNAs and specific protein components into Ataxin-2 granules. When taken together with other findings (Boeynaems *et al.*, 2021; Kim *et al.*, 2014; Satterfield & Pallanck, 2006; Singh *et al.*, 2021), our observations indicate that PAM2 binding to PABP on the polyA tail of mRNAs helps specify the composition of Ataxin-2 granules. We propose an early role for PAM2:PABP interactions working in coordination with the LSm domain to support mRNA translation and thereby oppose the mRNP formation (Boeynaems *et al.*, 2021); as well as a later role in escorting translationally-stalled PAM2:PABP linked mRNAs into mRNP granules. *In vivo* experiments analysing motor decline in transgenic *Drosophila* indicate that the PAM2:PABP interactions also support the progression of the neurodegenerative process. We provide new evidence for fresh insight into the enigmatic role of mRNP assembly in neurodegeneration.

RESULTS:

The structured PAM2 domain of Atx2 is necessary for the correct mRNA and protein content of Atx2 granules.

A recent eLife publication used Targets of RNA-Binding Proteins Identified by Editing (TRIBE) technology to identify mRNAs associated with Atx2 in the *Drosophila* adult brain

(Singh *et al.*, 2021). *In vivo*, the ability of an Atx2-fusion with ADARcd (the catalytic domain of an RNA-editing enzyme, ADAR), to edit a group of 256 target mRNAs was found to be dependent on the presence of the Atx2-cIDR, previously shown to be necessary for the formation of neuronal mRNP granules *in vivo*. In contrast, Atx2-ADARcd mutants lacking the LSm domain, both edited Atx2 TRIBE target RNAs and formed mRNP granules in cultured *Drosophila* S2 cells more efficiently than the wild-type. Thus, Atx2-ADARcd editing of target mRNAs occurs in and is reflective of mRNP granule assembly. While demonstrating a role for LSm-domain interactions in antagonizing cIDR mediated granule assembly, these observations did not address mechanisms by which Atx2 target mRNAs are selected, or whether and how Atx2 played any role in determining the composition of RNP granules. New experiments presented here address these outstanding questions.

Previous TRIBE analyses showed that LSm and LSm-AD regions have no major role in the recognition or selection of the Atx2-target mRNAs (Singh *et al.*, 2021). We therefore tested whether the third conserved region of Ataxin-2, a PAM2 motif known to associate with PABP (polyA binding protein), played any role in this process (Jiménez-López & Guzmán, 2014; Kaehler *et al*, 2012).

We used Gal80^{ts}-controlled *elav-Gal4* to express Atx2ΔPAM2-ADARcd (deleted for the PAM2 motif) in brains of adult *Drosophila* for 5 days and used RNA-Seq to identify edited RNAs in polyA selected brain mRNA and compare it with Atx2-ADARcd using procedures described earlier (Figure 1A) (McMahon *et al*, 2016). ADAR-edits, which converts Adenosine to Inosine on RNAs, are identified as A to G changes in TRIBE analyses. Each sample was sequenced to obtain 20 million reads (Supplementary table 1). The edits were only considered from the regions of the transcriptome that contained at least 20 reads. Genes with edits identified at a threshold above 15% in two biological replicates were considered as high-confidence true targets. We compared edit frequency and edited-gene identity in the brains of flies expressing Atx2ΔPAM2-ADARcd with those in brains expressing Atx2-ADARcd.

In contrast to Atx-2 forms lacking LSm or LSm-AD domains (Singh *et al.*, 2021), Atx2ΔPAM2-ADARcd edited significantly fewer RNA targets than wild-type Atx2-ADARcd (108 genes and 165 edits vs 256 genes and 317 edits, Figure 1B, C and Supplementary table 2). More striking, the cohort of mRNAs edited by the ΔPAM2 mutant form differed extensively from the largely overlapping cohorts edited by either wild-type forms of Atx2 (Figure 1C). Of

the 108 genes edited by Atx2ΔPAM2-ADARcd, 36 were also targets of Atx2-ADARcd, the remaining 72 were unique. (Figure 1C, D and Supplementary table 2). 50 edit sites were common between the Atx2ΔPAM2 and Atx2WT targets. Those sites were edited with much lower efficiency in Atx2ΔPAM2 as compared to Atx2WT (Figure 1E).

The location of edits made by Atx2ΔPAM2-ADARcd also differed dramatically as to where they occurred relative to the coding sequences of the target mRNAs (Figure 1F). While edits made by wild-type and ΔLSm forms of Atx2-ADARcd were greatly enriched in the 3'UTR of the mRNAs, Atx2ΔPAM2 targets were edited indiscriminately all along the mRNA length (Figure 1F).

Taken together, these data identify the PAM2 motif as necessary for Atx2 engagement with its correct mRNA targets. The PAM2 motif interacts with PABP, which binds polyA tracts at the 3' end of mRNAs (Deo *et al*, 1999). Therefore, the data point to a role for the structured PAM2:PABP interaction in guiding the association of Atx2 with mRNAs and for subsequent inclusion of these mRNAs in Atx2-containing granules.

If Atx2-ADARcd edits of target mRNAs occur predominantly in the mRNP granules (Singh *et al.*, 2021), then the ability of Atx2ΔPAM2-ADARcd to edit some target mRNAs would suggest that the PAM2 motif is not essential for mRNP granule formation *per se.* To examine this, we expressed wild-type and ΔPAM2 mutant forms of GFP-tagged Atx2 under control of the native genomic promoter in *Drosophila* S2R+ cells. Atx2 overexpression in S2 cells induced the formation of mRNP granules closely related to SGs, containing endogenous Atx2 and various SG proteins as previously reported (Figure 2A) (Bakthavachalu *et al.*, 2018; Singh *et al.*, 2021). Similar expression of Atx2ΔPAM2-GFP also induced granule formation. However, these granules were compositionally distinct from those induced by Atx2-GFP. While they clearly contained some SG markers present on Atx2-granules, e.g., Me31B and Rox8 (*Drosophila* homologs of DDX6 and TIA1), they did not contain others such as PABP, Caprin and dFMRP (Figure 2B).

RNP-granules induced by expression of wild-type, LSm and PAM2 deficient forms of Atx2-GFP required the presence of the c-terminal IDR (Figure 2C). Thus, while largely dispensable for efficient mRNP assembly, the PAM2 domain plays a significant role in determining both mRNA and protein components of mRNP granules. One possibility is that the PAM2 motif

directly recruits PABP and associated mRNAs to granules and indirectly recruits other proteins through their interactions with either PABP or mRNAs brought to RNP granules through Atx2-PAM2:PABP interactions.

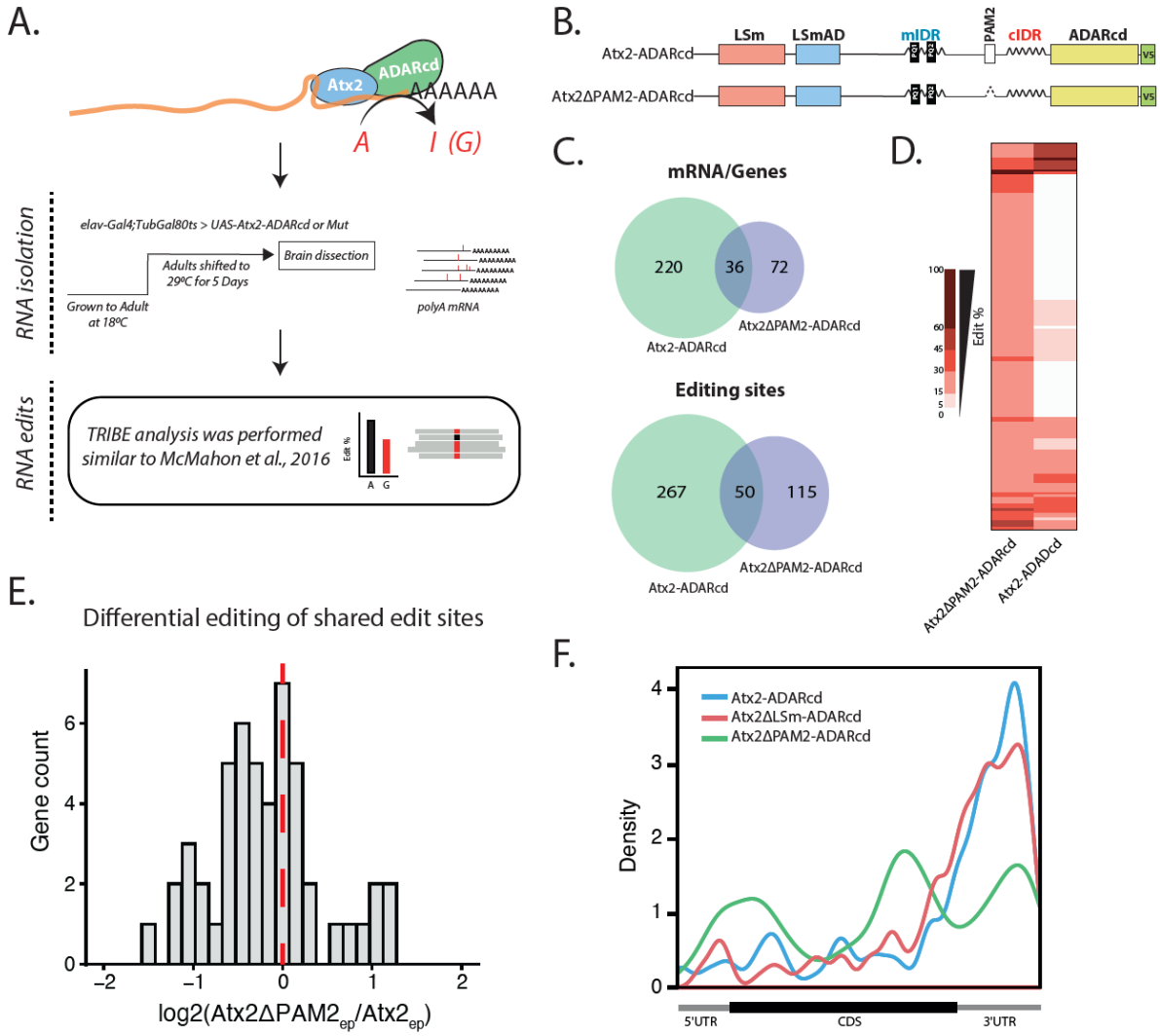

Figure 1: The PAM2 domain facilitates the selection of Atx2 RNA targets. (A). Flowchart depicting the TRIBE analyses pipeline. Atx2ΔPAM2-ADARcd was expressed in adult *Drosophila* brains. Total brain RNA was isolated and RNA edits were identified and compared to Atx2-ADARcd, similar to Singh et al 2021. (B) Domain map of Atx2-ADARcd constructs used for TRIBE analysis. (C) Comparisons of genes and edits identified by TRIBE between Atx2-ADARcd and Atx2ΔPAM2-ADARcd targets. (D) Most Atx2ΔPAM2 targets identified by TRIBE are unique and not edited in Atx2WT, suggesting that these new targets bound by Atx2ΔPAM2 are not native Ataxin-2 granule targets. (E) Comparisons of the editing efficiency ratio of common edits between Atx2WT vs Atx2ΔPAM2 show a much lower editing efficiency in Atx2ΔPAM2 compared to Atx2WT. (F) PAM2 deletion results in loss of 3'UTR specificity seen in Atx2WT and LSm deletion TRIBE target mRNAs. Atx2WT and Atx2ΔLSm-ADARcd data are extracted from (Singh et al 2021).

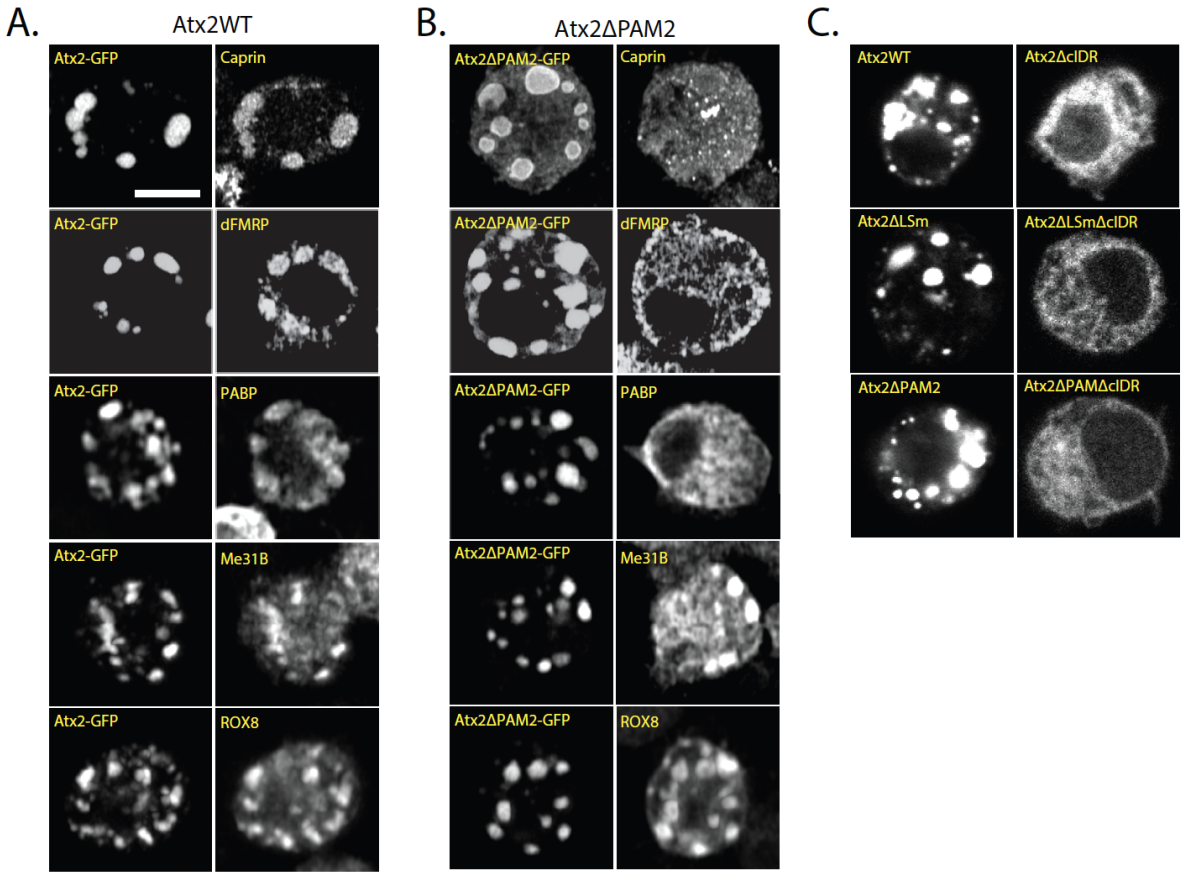

Figure 2: Presence of the PAM2 domain affects the protein composition of Atx2-GFP granules in S2 cells. (A) Over-expression of Atx2-GFP in unstressed *Drosophila* S2 cells induces the formation of Atx2-GFP granules to which various SG markers co-localize. (B) Deletion of the PAM2 affects the Atx2-GFP granule composition. Over-expression of Atx2ΔPAM2-GFP in S2 cells still induces the formation of granules, but some SG markers fail to co-localize in these, notably dFMR, Caprin and PABP. (C) Atx2-GFP granule formation in S2 cells relies primarily on the cIDR. Deletion of the cIDR in Atx2WT, Atx2ΔPAM2 and Atx2ΔLSm, removes their ability to form granules upon overexpression. See Supplemental Figure 1, A-B, for quantification. The scale bar in (A) applies to (B) and (C). Scale bar = 5 µm,

PAM2:PABP interactions are sufficient for Atx2 to associate with stress granules

We wanted to directly confirm Ataxin-2 PAM2 motif interactions with PABP and analyse their relevance to RNP granule assembly. For this, we generated constructs encoding SNAP-epitope tagged variants of Atx2. These were radically truncated forms of *Drosophila* and human Ataxin-2 proteins containing only the LSm, LSm-AD and PAM2 elements and lacking all unstructured regions of the protein. The structured elements are connected via flexible linkers (Figure 3A). These "Mini-Ataxin-2" constructs and their domain-deleted forms allowed us to separate functions of the structured regions of Ataxin-2 from those of the remaining extended

disordered regions. A similar approach has been previously shown for MeCP2 (Tillotson *et al*, 2017). We identified key residues involved in *Drosophila* Atx2-PAM2:PABP interactions based on a previously solved crystal structure of a strongly conserved mammalian PAM2:PABPC1-MLLE domain complex (Kozlov *et al*, 2010; Xie *et al*, 2014) (Figure 3B). Residues leucine 914 and phenylalanine 921 (L914 and F921) in the human ATXN2-PAM2 motif are predicted to contact the PABPC-MLLE domain and of these, F921 has been shown to be required for the PABPC-ATXN2 interaction (Inagaki *et al*, 2020). These residues (L859 and F866, respectively) are perfectly conserved in fly Atx2 (Supplementary Figure 3). In order to allow more precise disruption of PAM2:PABP interactions and avoid potential unknown secondary effects of larger PAM2 motif deletions, we additionally generated mini Ataxin-2 constructs where these PABP-contacting residues were singly or doubly altered to alanine. We used these constructs for co-immunoprecipitation (Figure 3) and co-localization (Figure 4) analyses to examine the contribution of PAM2:PABP/PABPC1 interactions in RNP-granule formation.

We expressed SNAP-tagged wild-type and mutant forms of mammalian and *Drosophila* mini-Ataxin-2 in HEK293T and S2 cells, respectively. We tested which Ataxin-2 domains were required for SNAP substrate beads to successfully immunoprecipitate Ataxin-2 complexes containing PABPC1/PABP from cell lysates (Figure 3C-E). Both LSM12 and PABPC1 proteins were co-immunoprecipitated with mammalian mini-ATXN2. However, PABPC1 co-immunoprecipitation was selectively lost when the PAM2 domain was deleted or if predicted PABP-contact residues in the PAM2 domain were mutated (Figure 3C). Similar to the human homolog, fly mini-Atx2-SNAP also required the presence of its PAM2 motif with both predicted contact residues intact for immunoprecipitation of PABP from *Drosophila* S2 cell lysates (Figure 3D). Taken together with previous observations, these data support a potential sequence of molecular events. In unstressed cells, PAM2 domain interaction with PABP help position Ataxin-2 at the 3'-end of mRNAs while LSM-domain association with LSM12 stimulate translation of these mRNAs; under stress conditions (or Ataxin-2 overexpression), translation is arrested and the cIDR domain freed to mediate interactions that facilitate the formation of condensed RNP granules (see Discussion)

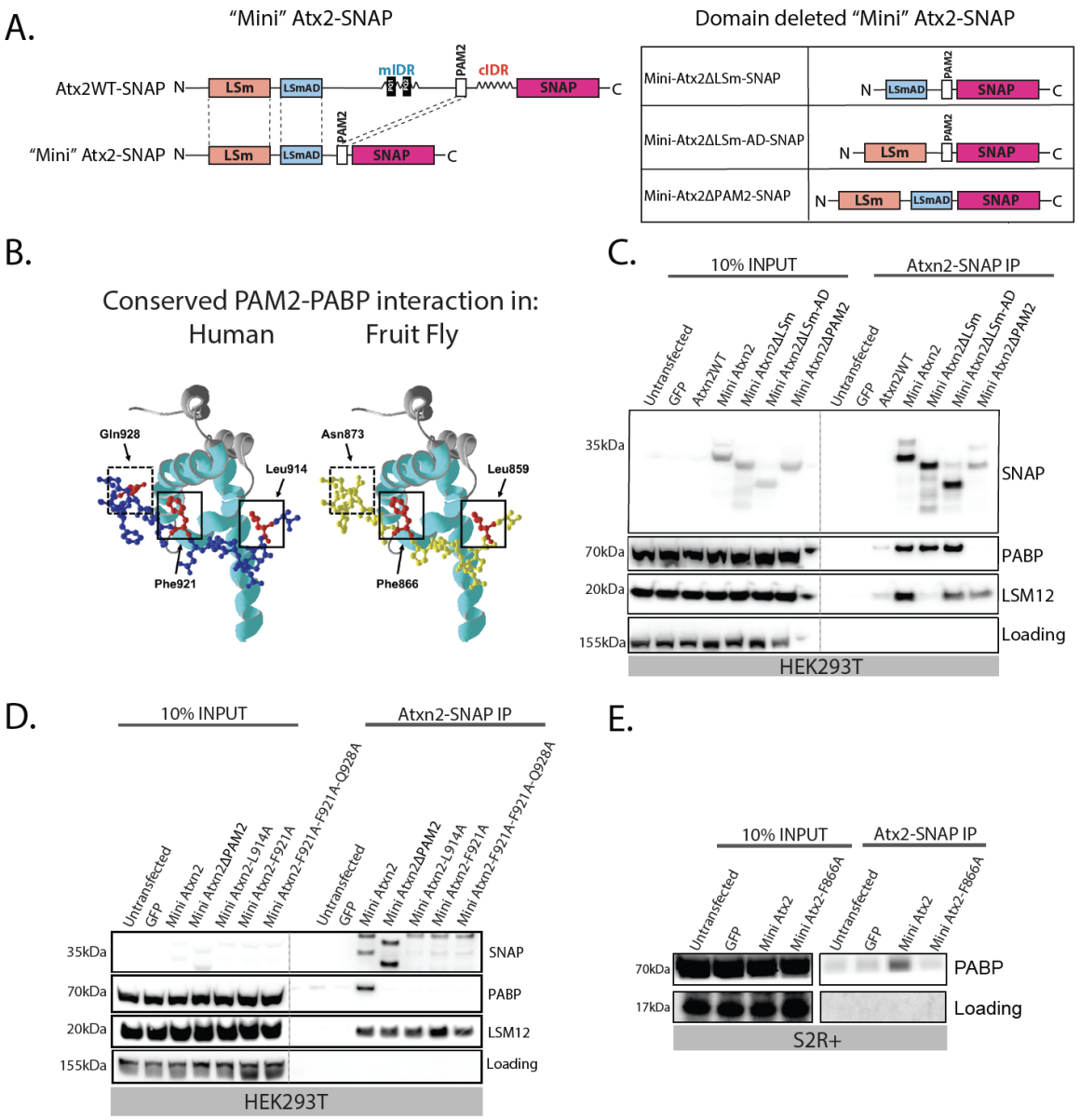

Figure 3: A minimized Ataxin-2 construct containing only the known structured domains maintains the ability to interact with PABP and LSM12. (A) Schematic of SNAP-tagged full length, minimal, and minimal domain-deleted constructs of fly Atx2 used to isolate the function of the structured domains of the protein without interference from IDR-mediated interactions. Human and *Drosophila* Ataxin-2 LSm, LSm-AD and PAM2 domains show high amino acid sequence similarity (Clustal Ω) of 70%, 82% and 87% respectively. This suggests conserved and specific function of these structured domains. (B) Structural model of the PABP MLLE domain (ribbon) showing the near-perfect structural similarity of the human ATXN2 PAM2 domain (blue, uniprot ID: Q99700) with the *Drosophila* Atx2 PAM2 domain (yellow, uniprot ID: Q8SWR8). The key interacting residues are highlighted in red. (C) Human minimized ATXN2 SNAP IP-WB from HEK293T cells probing for PABP and LSM12 showing the effects of different domain deletions. The PAM2 domain is necessary and sufficient for the ATXN2-PABP interaction, while the LSm domain is necessary and sufficient for the ATXN2-LSM12 interaction. (D) Point-mutations targeting key interacting residues of the PAM2 domain were predicted to replicate the

effect of a full PAM2 deletion in the minimized Atx2 construct. Human minimized ATXN2-SNAP IP WB from HEK293T cells showing that mutating either of the key hydrophobic residues L914 or F921 in the PAM2 domain is sufficient to prevent its interaction with PABP. The interaction with LSM12 is unaffected by the point mutations. (E) *Drosophila* minimized Atx2-SNAP IP-WB from S2 cells. An analogous PAM2 domain point mutation on F866 blocks the Atx2-PABP interaction.

Single mRNAs usually associate with multiple PABP molecules because their polyA tails are considerably longer than the ~24 bases required for PABP binding (Mangus *et al*, 2003). Thus, in cells expressing endogenous and mini Ataxin-2, mRNAs could have both forms associated with their polyA tails. In response to stress, mini Ataxin-2 would be expected to move into SGs whose formation is facilitated by IDRs on endogenous Ataxin-2 associated with the common target RNAs. We examined this possibility in cells before and after oxidative stress.

Drosophila and human mini-Ataxin-2-SNAP, expressed in fly S2 or human U2OS cells respectively, were diffusely localized in the cytoplasm and neither induced formation of Ataxin-2 foci. However, when cells were exposed to sodium arsenite to induce SG formation, SNAP-tagged mini-Atx2 (Figure 4A) and mini- ATXN2 (Figure 4H) were robustly recruited to stress granules. Thus, association of Ataxin-2 with mRNP-granule components may be achieved by structured domain interactions alone, independently of IDRs required for mRNP assembly into granules.

Further experiments examined which of the LSm, LSm-AD and/or PAM2 domains were necessary for mini-Ataxin-2 to associate with stress granules. Mammalian and *Drosophila* mini-Ataxin-2 forms missing the LSm or LSm-AD domains could still be found in stress granules (Figure 4B-C and I-J). In contrast, mutants lacking the PAM2 domain remained cytoplasmic after stress in both S2 (Figure 4D) and U2OS cells (Figure 4K). Notably, point mutations in the Ataxin-2-PAM2 domain that specifically disrupt PAM2:PABP interaction similarly prevent localization to stress granules (Figure 4E-G and L-N). Thus, interactions between Ataxin-2's PAM2 domain and PABP appear important for the presence of Ataxin-2 in native mRNP granules, whose assembly is driven by the distinct (IDR) region of the protein (Figure 2C). The ability of otherwise full-length Ataxin-2 lacking PAM2 to form compositionally distinct mRNP assemblies (Figure 2B) suggests that PAM2:PABP binding also serves to limit non-physiological interactions by Ataxin-2 (See Discussion).

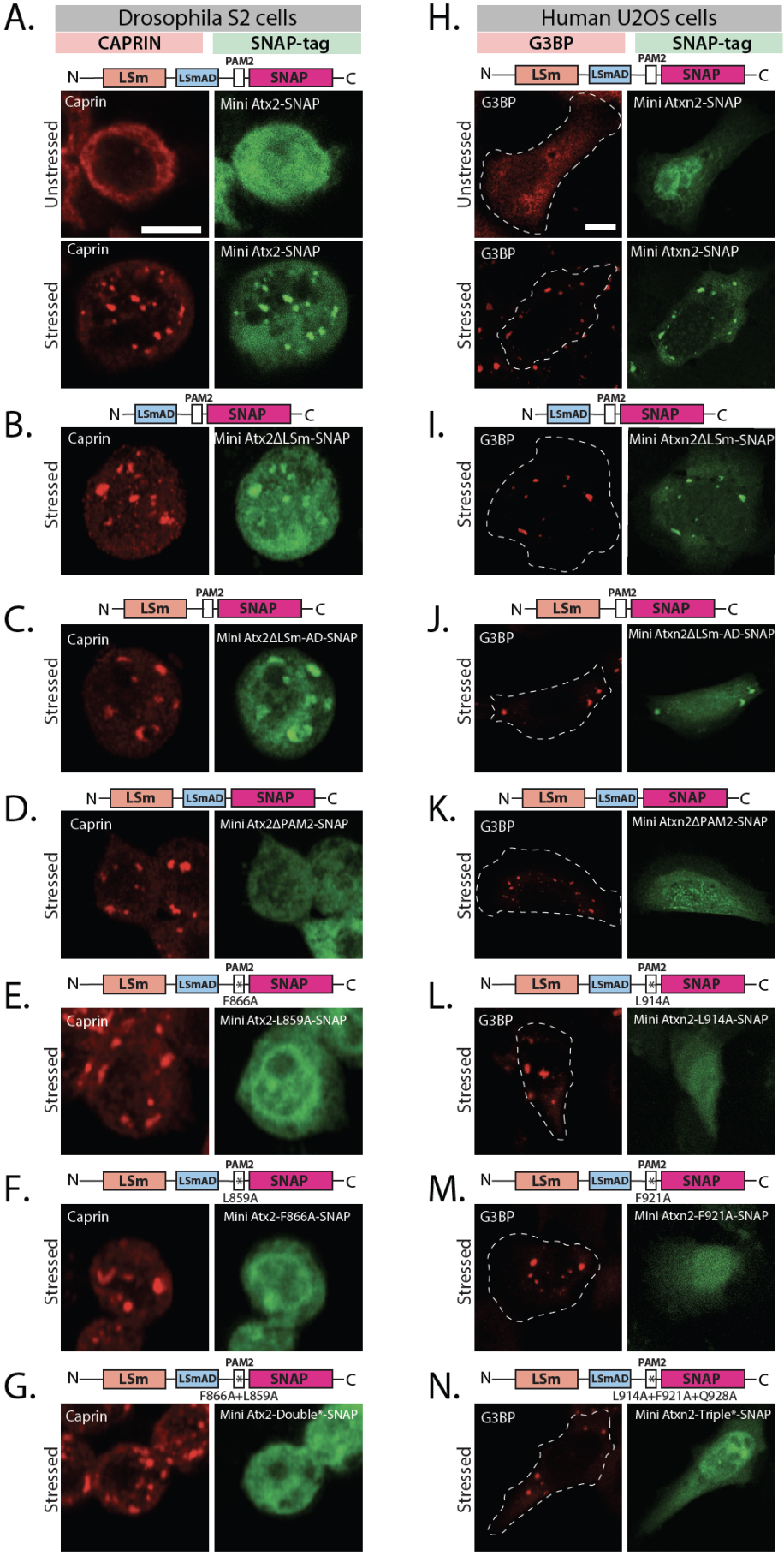

334

Figure 4: **The structured PAM2 domain is necessary and sufficient for Ataxin-2 recruitment to Stress Granules in both *Drosophila* and human cells.** (A) In *Drosophila* S2 cells mini-Atx2-SNAP (green) is recruited to SGs induced by arsenite. (B) Deletion of LSm or (C) LSm-AD domains has no significant effect in the arsenite-induced SG recruitment. (D) The presence of PAM2 domain, and specifically its key PABP-interacting amino acids (E-G), is necessary for Atx2 recruitment to SGs. Caprin (red) was used as SG granule marker, scale bar = 5 μm, (H) Human mini-ATXN2-SNAP (green) is recruited to arsenite-induced SGs in human U2OS cells. (I) Deletion of LSm or (J) LSm-AD domains has no effect on the arsenite-induced SG recruitment of ATXN2. (K) Deletion of the PAM2 domain, and specifically its PABP-interacting amino acids (L-N), are necessary for ATXN2 recruitment to SGs. G3BP1 (red) was used as SG marker; scale bar = 10 μm. Schematics above images indicate the domain deletions or amino acid mutations that were made in the different Ataxin-2 constructs. See Supplemental Figure 1C for quantification.

The IDR and PAM2 domains promote and the LSm domain inhibits cytotoxicity in Drosophila neurodegeneration models.

Three different Ataxin-2 domain deletions tested showed three distinct effects on mRNP granule assembly in S2 cells. IDR domain deletions prevent Ataxin-2 granule formation. LSm-domain deletion enhances the formation of Ataxin-2 granules. PAM2 domain deletions result in the formation of unusual mRNP assemblies (Bakthavachalu *et al.*, 2018; Singh *et al.*, 2021) (Figure 2B/C). Prior observations showing that Atx2 IDR deletions suppress cytotoxicity in *Drosophila* models for neurodegeneration indicate that mRNP granules support events that lead to degenerative disease (Bakthavachalu *et al.*, 2018; Becker *et al.*, 2017; Huelsmeier *et al.*, 2021; Scoles *et al.*, 2017). If true, the expression of Atx2ΔLSm, which enhances granule assembly, would promote or potentially accelerate the degeneration, while the expression of Atx2ΔcIDR would not. The expression of Atx2ΔPAM2 would be expected to support mRNP assemblies of different compositions from the ones containing wild-type or ΔLSm forms of Atx2. The effects on degeneration for this condition would be hard to predict.

To examine how the different Atx-2 domain deletions affect nervous system integrity and function over time, we combined a Gal4-responsive *UAS-Atx2* transgene with *elav-Gal4* and *TubGal80^{ts}*. This allows us to use a temperature shift from 18ºC to 30ºC to induce *UAS-Atx2* transgene expression, specifically in the brains of adult flies (Figure 5A). We then analysed the rate at which flies climbed the walls of a glass cylinder, a surrogate measure of motor ability, one day and 15 days after transgene expression. All genotypes tested showed robust and

370 comparable levels of climbing ability on day 1. Interesting variations were identified on day
371 15. The 15-day old flies expressing Atx2WT or Atx2ΔLSm showed a strong decline in
372 climbing ability. In contrast, Atx2 ΔcIDR flies showed a minimal decline (Figure 5B). These
373 observations were in line with the effects of these Atx2 types on granule formation. Strikingly,
374 flies expressing the Atx2ΔPAM variant, which formed compositionally distinct granules in S2
375 cells, showed no significant decline in climbing ability, suggesting that Atx2's ability to
376 promote progressive decline of neural function depends less on Atx2 granule formation and
377 aggregation, but a bit more on its sequestration of critical translation factors such as PABP (and
378 associated RNAs.(Figure 5B). These observations support and extend prior work showing that
379 heterologous overexpression of full-length, but not PAM2-domain deleted forms of
380 mammalian ATXN2 enhances mammalian TDP-43-induced degeneration of the *Drosophila*
381 compound eye (Kim *et al.*, 2014). They are also consistent with work in mice showing that
382 PABPC1 sequestration in inclusions correlates strongly with the progression of
383 neurodegeneration (Damrath *et al*, 2012).
384
385 The conclusion, that PAM2 mediated interactions were required for progressive cytotoxicity,
386 is further supported by a parallel series of experiments in which we used *mef2-Gal4* in place
387 of *elav-Gal4,* to *target UAS-Atx2* transgene expression to *Drosophila* adult muscles (Figure
388 5C). Micro-computed tomography (micro-CT) scanning to visualize the integrity of flight
389 muscle fibers in whole-mount preparations (see Methods) revealed degeneration of muscles
390 expressing wild-type Atx2 in 20-day old flies. While there was more severe degeneration in
391 Atx2ΔLSm expressing muscle, muscles similarly expressing Atx2ΔcIDR or Atx2ΔPAM forms
392 showed no morphological defects (Figure 5C and Supplementary Figure 4).

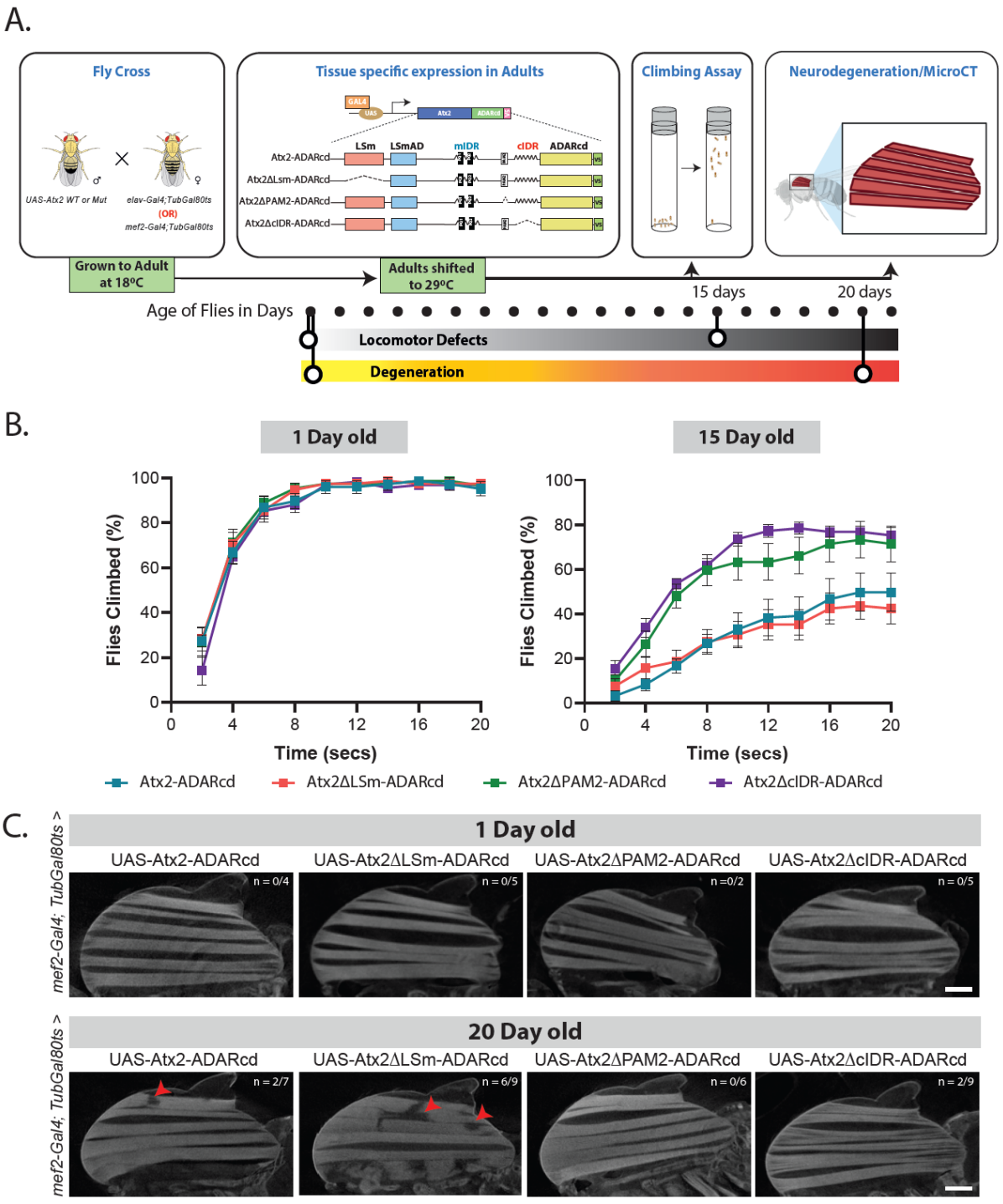

Figure 5: The IDR and PAM2 domains promote and the LSm domain inhibits neurodegeneration in *Drosophila*. (A) A schematic of the experimental design is shown. UAS-transgenes were crossed with *elav-Gal4; tub-Gal80^{ts}* or *mef2-Gal4, tub-Gal80^{ts}* and kept at 18°C till the adult flies emerged. The flies were shifted to 29 °C for days shown with dots under the experimental design. Fly climbing or indirect flight muscle cytotoxicity was studied. (B) *Drosophila* climbing behavior assay was performed by driving UAS-transgene (Atx2WT, Atx2ΔcIDR, Atx2ΔPAM or Atx2ΔLSm) with *elav-Gal4.* A graph was plotted with number of flies (Y-axis) that crossed the 20ml mark at a given time (X-axis). (C) Cellular toxicity was measured by driving UAS-transgene (Atx2WT, Atx2ΔcIDR, Atx2ΔPAM or Atx2ΔLSm) with *mef2-*

Gal4. Fly indirect flight muscles were imaged using micro-CT and the loss of muscle fibers is shown with solid red arrowheads.

DISCUSSION

The results described above provide three significant lines of insight. First, they support a detailed model for sequential protein-protein interactions through which Ataxin-2 can modulate different translational states of a single mRNA. Second, they show that the Ataxin-2 polypeptide contains distinct activities that promote or protect against neurodegeneration, pointing to the value of developing therapeutics that target specific Ataxin-2 interactions, beyond those that reduce overall levels of the protein. Third, the work identifies a novel molecular mechanism involving the PAM2 domain and PABP that contributes to the assembly of mRNP granules.

Molecular mechanisms of Ataxin-2 function

Some RNA-binding proteins can remain associated with mRNAs across multiple stages: RNA processing, transport, translation, or translational control (Formicola *et al.*, 2019; Gomes & Shorter, 2019; Hachet & Ephrussi, 2004; Harlen & Churchman, 2017; Lin *et al*, 2015; Maniatis & Reed, 2002). Ataxin-2 may be one such protein. It is a translational activator of the *Drosophila period* mRNA, a repressor of several miRNA reporters, a facilitator of neuronal mRNP-granule and stress-granule formation as well as a broad stabilizer of Ataxin-2 associated mRNAs (Bakthavachalu *et al.*, 2018; Inagaki *et al.*, 2020; Lim & Allada, 2013; McCann *et al*, 2011; Nonhoff *et al*, 2007; Sudhakaran *et al*, 2014; Yokoshi *et al*, 2014; Zhang *et al*, 2013). While these different functions could represent different modes of engagement with distinct sets of mRNAs, the data are also consistent with another model. Sequential interactions mediated by different protein regions during mRNP modelling allow Ataxin-2 to contribute in multiple ways to translational control to a single mRNA.

Previous work has shown that Atx-2 enhances *period* mRNA translation through a mechanism requiring LSm-domain interactions with a complex of LSM12 and TYF (Twenty Four) proteins associated with the 5'cap of the translating mRNA (Lee *et al*, 2017; Lim & Allada, 2013; Zhang *et al.*, 2013). Given considerable supportive evidence for direct binding between the LSm-domain and LSM12, we postulate that LSm-domain-LSM12 interactions occur in translating polysomes (Satterfield & Pallanck, 2006) and contribute to increased efficiency of translation.

This proposal is consistent with the observation that the LSm domain opposes the formation of mRNP granules, which usually contain translationally repressed mRNAs (Singh *et al.*, 2021).

However, the LSm domain must also contribute to LSM12-independent functions, because while LSm-domain deletions from *Drosophila* Atx2 cause lethality and LSM12 null mutants, while arrhythmic, are viable and fertile (Lee *et al.*, 2017). One possibility is that LSm domains additionally contribute, perhaps indirectly, to interactions with the DEAD-box helicase Me31B/DDX6 in a translational repressor complex (Brandmann *et al*, 2018; Lee *et al.*, 2017). Thus, we suggest that in the case of actively translating mRNAs, the Atx2 function is driven by LSm-domain association with LSM12 and translational initiators, and that LSM12 disengages from a translational initiation complex as the mRNA transitions into a repressed state driven by Me31B.

While polyA tails and PABP are known to support translation and the Ataxin-2 PAM2 domain is involved in targeting the protein to polysomes (Satterfield and Pallanck, 2006), existing data do not directly address how Ataxin-2 PAM2 motif interactions contribute to translational activation. One possibility, supported by observations on the *period* mRNA is that the PAM2-domain guides Ataxin-2 to the 3'UTR of its target mRNAs (Lim & Allada, 2013). Our observation that PABP co-immunoprecipitates with mini-Ataxin2, show that Atx2-PAM2:PABP interactions occur independently of and prior to mRNP granule formation. Recent findings that this association antagonizes the Ataxin-2 condensation (Boeynaems *et al.*, 2021) are consistent with a model in which the Atx2-PAM2 motif interacts with PABP in translating mRNAs to support efficient translation driven by the LSm-LSM12 complex. However, in addition to supporting translation, PABP is also known to associate with translational repressors that could drive either mRNA deadenylation and/or storage (Machida *et al*, 2018; Yoshida *et al*, 2006). Our data support such a dual role for Ataxin-2 associated with PABP in translational repression. First, when Ataxin-2 target mRNAs are not actively translated, then the mRNP through Me31B/DDX6 and PABP may recruit deadenylases to transition into either a translationally dormant or degradative state (Lee *et al.*, 2017; Machida *et al.*, 2018; Yi *et al*, 2018; Yoshida *et al.*, 2006). Second, Atx2 associated mRNA may move into mRNP granules whose formation is facilitated by Atx2 IDR-mediated condensation. We postulate that mRNAs in such assemblies are stored in a form that is protected from degradation. While the above model, shown in Figure 6, is consistent with all our data, we

acknowledge that it needs extensive and rigorous testing in the context of the life cycle of a single Ataxin-2 target mRNA.

Implications for Ataxin-2 as a therapeutic target

Antisense Oligonucleotide (ASO) based therapeutic strategies that lower levels of Atxn-2 are being developed for the treatment of ALS and spinocerebellar ataxia type 2 (SCA2) (Becker *et al.*, 2017; Scoles *et al.*, 2017). Our experiments provide a much finer grained analysis of activities of Ataxin-2, suggesting that the function of the LSm domain should be spared, and that IDR mediated assembly mechanisms and perhaps PAM2:PABP interactions should be most usefully targeted by therapeutics.

Our previous work showed that *Atx2* mutants lacking the cIDR required for Ataxin-2 granule formation in Drosophila neurons and S2 cells, were resistant to neurodegeneration as assessed in *Drosophila* disease models (Bakthavachalu *et al.*, 2018; Huelsmeier *et al.*, 2021). We further showed that the LSm-domain antagonizes Ataxin-2 granule formation (Singh et al, 2021). Here we advance the latter observation by demonstrating that Ataxin-2 forms lacking the LSm domain may more effectively cause cytotoxicity than the wild-type or IDR-deficient forms (Figure 5C). These observations independently confirm our original conclusions and-provide further support for a model in which the efficiency of mRNP assembly correlates with the speed and severity of neurodegenerative processes in *Drosophila*.

The importance of the PAM2 domain in promoting degeneration has been previously observed by experiments showing that heterologous expression of a pathogenic form of human Ataxin-2 lacking its PAM2 domain, but not the full-length form, suppresses cytotoxicity in *Drosophila* expressing human TDP-43 (Kim *et al.*, 2014). Our observations that expression of Atx2ΔPAM2 is far less toxic than expression of wild-type Atx2 is consistent with this. In addition, by showing that Atx2ΔPAM2 forms compositionally different Ataxin-2 granules, they highlight the importance of specific granule components, and not granules *per se,* in neurodegenerative pathologies. Thus, while liquid-liquid transitions mediated by disordered domains could be a shared requirement for the formation of multiple types of mRNP granules, we speculate that each granule type, with distinctive composition, could preferentially support one or other type of proteinopathy (De Graeve & Besse, 2018; Vogler *et al*, 2018).

Structured interactions may determine mRNP granule composition.

Many lines of evidence argue that specific molecular interactions, e.g. mediated by structured domains of the P-body component Edc3 or the stress-granule components G3BP and Caprin, contribute to the mRNP granule formation (Decker *et al.*, 2007; Kedersha *et al*, 2016). In engineered systems, the condensation of RNA-binding proteins and mRNAs into granules has been clearly shown to depend on both traditional protein-protein interactions and on more promiscuous interactions between intrinsically disordered regions (Protter *et al*, 2018). Our work now identifies the interactions between Ataxin-2's PAM2 motif and PABP as a critical contributor to the assembly of Ataxin-2 containing mRNP granules. This suggests a mechanism by which the interaction helps select mRNA and protein components of mRNP granules.

We suggest that Ataxin-2, guided by PAM2:PABP interactions and LSm domain interactions, recruits target mRNAs and associated proteins into translating mRNPs (Satterfield & Pallanck, 2006). Under conditions where the translation is arrested, LSm-domain interactions are altered (Lee *et al.*, 2017), and transcripts are released from stalled ribosomes. Base-pairing interactions between exposed mRNA side chains, as well as interactions between Ataxin-2's now accessible intrinsically disordered regions, contribute to the assembly of these mRNPs into granules. This logical sequence of events is consistent with: (a) TRIBE data showing a reduced number of edits of native Ataxin-2 target mRNAs by Atx2ΔPAM2-ADARcd; (b) the inability of ΔPAM2-miniAtx2 constructs to associate with stress granules; and (c) the aberrant protein composition of granules induced by Atx2ΔPAM2 in S2 cells. The additional observation that Atx2ΔPAM2-ADARcd expression results in a large number of non-native mRNA edits, indicates that the PAM2:PABP interaction not only selects correct target mRNAs but also prevents Ataxin-2 engagement with incorrect mRNA target regions.

Our conclusion that Ataxin2-PAM2:PABP interactions are involved in the selection of mRNA components of RNP granules is superficially inconsistent with the observation that RNA components of native stress granules can be predicted with remarkable accuracy on the basis of mRNA size. This argues for a primary role for RNA-RNA interactions in the stress granule assembly (Jain & Vale, 2017; Matheny *et al.*, 2021; Van Treeck & Parker, 2018). However, we note that experiments presented here do not address mechanisms by which mRNAs are selected into stress granules. Instead, the TRIBE data address how Atx2-target mRNAs are selected into neuronal mRNP granules that exist in non-stressed cells *in vivo*, and microscopic studies analyse protein components of mRNP granules formed following Atx2 expression in S2 cells. Our experiments and observations therefore point to fundamental differences in

mechanisms by which the assembly of neuronal granules, or granule types found in unstressed cells, may differ from those involved in stress-granule assembly. The regulation and composition of the former class could well rely extensively on specific protein-protein and protein-mRNA interactions, which may be revealed by future analyses of mechanisms by which such mRNP assemblies are formed *in vivo*.

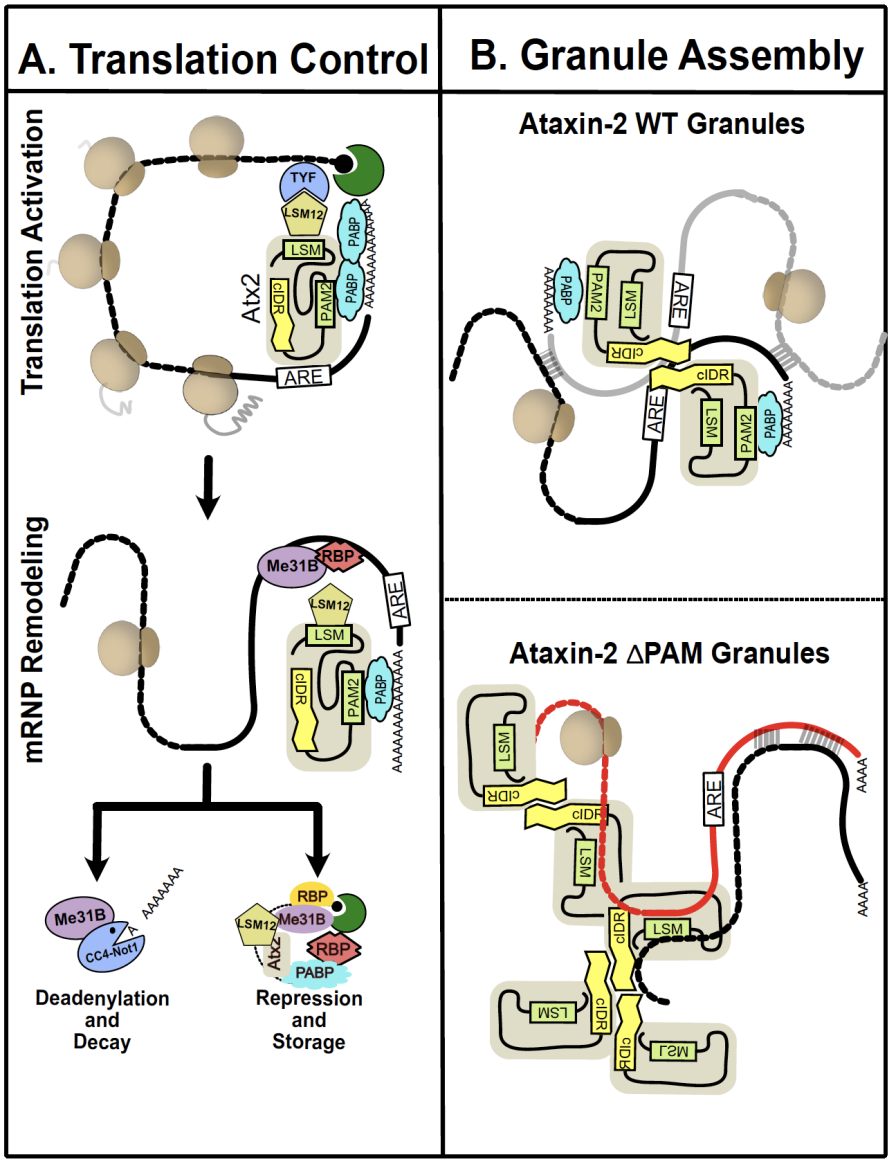

Figure 6: A model for Ataxin-2 RNP dynamics and the role of PAM2 domain in determining its RNP composition and mRNA selection. (A) Ataxin-2 is recruited to mRNAs by RBPs during different stages of the mRNA life cycle. Ataxin-2 activates translation of subsets of mRNA by recruiting LSM12, TYF and other translation activation complexes. Under specific conditions, mRNP remodelling exposes Ataxin-2 cIDR that mediates multivalent interactions and RNP granule assembly. Ataxin-2 recruits Me31B and CCR4-NOT1 complexes that lead to deadenylating and/or translation repression. It is possible that LSM12/TYF continue to associate with RNA but are probably not part of repressor complexes. RNA

551 deadenylation can lead to degradation or translation repression and storage in RNP granules. (B) Ataxin-
552 2-PAM2 domain determines protein and RNA partners of the RNP granules. PAM2 domain is essential for
553 recruitment of Ataxin-2 to stress granules that also contains other RBPs (eg. Me31B, FMRP, Rox8, Rin
554 and Caprin). Ataxin-2-cIDR along with RNA-RNA interaction stabilise the stress induces RNP
555 condensation. In the absence of the PAM2 domain, Ataxin-2 fails to recruit specific target mRNA and
556 proteins. Remodelling of Ataxin-2 exposes the cIDR to induce phase separation and aberrant RNP
557 condensation. The Ataxin-2ΔPAM2 granules are non-toxic and lack several known stress granule proteins
558 (eg.FMRP, Caprin and PABP).
559

Materials and methods

Key resources table

Reagent type (species) or resource	Designation	Source or reference	Identifiers	Additional information
Genetic reagent (*Drosophila melanogaster*)	*UAS-Atx2-WT-ADARcd*	Singh *et al.* 2021	N/A	
Genetic reagent (*Drosophila melanogaster*)	*UAS-Atx2-ΔLSm-ADARcd*	Singh *et al.* 2021	N/A	
Genetic reagent (*Drosophila melanogaster*)	(*UAS-Atx2- ΔPAM2-ADARcd*)	This paper	N/A	
Genetic reagent (*Drosophila melanogaster*)	*UAS-Atx2- ΔcIDR-ADARcd*	Singh *et al.* 2021	N/A	
Genetic reagent (*Drosophila melanogaster*)	*UAS-Atx2-only LSm/Lsm-AD - ADARcd*	Singh *et al.* 2021	N/A	
Genetic reagent (*Drosophila melanogaster*)	*mef2-Gal4; Tub-Gal80^{ts}*	Bloomington *Drosophila* Stock center	Derived from #50742	
Genetic reagent (*Drosophila melanogaster*)	*elav-Gal4; Tub-Gal80^{ts}*	Bloomington *Drosophila* Stock center	Derived from #458	
Cell line (Drosophila melanogaster)	S2R+ cells	DGRC	RRID:CVCL_Z831	
Cell line (Human)	HEK293T	Gift: Adrian Bracken lab	N/A	
Cell line (Human)	U2OS	Gift: Martina Schroeder lab	N/A	
Recombinant DNA reagent	pUASt-Atx2-SNAP_fly (Plasmid)	This paper	N/A	Construct to express fly Atx2WT -SNAP
Recombinant DNA reagent	pUASt-ATXN2-SNAP_hum (Plasmid)	This paper	N/A	Construct to express human WT ATXN2-SNAP
Recombinant DNA reagent	pUASt-mini-Atx2-SNAP_fly (Plasmid)	This paper	N/A	Construct to express fly mini Atx2-SNAP
Recombinant DNA reagent	pUASt-mini-ATXN2-SNAP_hum (Plasmid)	This paper	N/A	Construct to express human mini ATXN2-SNAP
Recombinant DNA reagent	pUASt-ΔLSm-mini-Atx2-SNAP_fly (Plasmid)	This paper	N/A	Construct to express fly ΔLSm mini Atx2-SNAP
Recombinant DNA reagent	pUASt-ΔLSm-mini-ATXN2-SNAP_hum (Plasmid)	This paper	N/A	Construct to express human ΔLSm mini ATXN2-SNAP
Recombinant DNA reagent	pUASt-ΔLSmAD-mini-Atx2-SNAP_fly (Plasmid)	This paper	N/A	Construct to express fly ΔLSm-AD mini Atx2-SNAP
Recombinant DNA reagent	pUASt-ΔLSmAD-mini-ATXN2-SNAP_hum (Plasmid)	This paper	N/A	Construct to express human ΔLSm-AD mini ATXN2-SNAP
Recombinant DNA reagent	pUASt-ΔPAM2-mini-Atx2-SNAP_fly (Plasmid)	This paper	N/A	Construct to express fly ΔPAM2 mini Atx2-SNAP
Recombinant DNA reagent	pUASt-ΔPAM2-mini-ATXN2-SNAP_hum (Plasmid)	This paper	N/A	Construct to express human ΔPAM2 mini ATXN2-SNAP

Recombinant DNA reagent	pUASt-L859A-mini-Atx2-SNAP_fly (Plasmid)	This paper	N/A	Construct to express fly PAM2* L859A mini Atx2-SNAP
Recombinant DNA reagent	pUASt-L914A-mini-ATXN2-SNAP_hum (Plasmid)	This paper	N/A	Construct to express human PAM2* L914A mini ATXN2-SNAP
Recombinant DNA reagent	pUASt-F866A-mini-Atx2-SNAP_fly (Plasmid)	This paper	N/A	Construct to express fly PAM2* F866A mini Atx2-SNAP
Recombinant DNA reagent	pUASt-F921A-mini-ATXN2-SNAP_hum (Plasmid)	This paper	N/A	Construct to express human PAM2* F921A mini ATXN2-SNAP
Recombinant DNA reagent	pUASt-L859A-F866A-mini-Atx2-SNAP_fly (Plasmid)	This paper	N/A	Construct to express fly PAM2* L859A and F866A mini Atx2-SNAP
Recombinant DNA reagent	pUASt-L914A-F921A-Q928A-mini-ATXN2-SNAP_hum (Plasmid)	This paper	N/A	Construct to express human PAM2* L914A, F921A and Q928A mini ATXN2-SNAP
Recombinant DNA reagent	pAcman-Atx2-GFP (Fosmid)	Sudhakaran et al. 2013	N/A	Genomic construct to express fly WT Atx2-GFP
Recombinant DNA reagent	pAcman-ΔLSm-Atx2-GFP (Fosmid)	This paper	N/A	Genomic construct to express fly ΔLSm Atx2-GFP
Recombinant DNA reagent	pAcman-ΔPAM2-Atx2-GFP (Fosmid)	This paper	N/A	Genomic construct to express fly ΔPAM2 Atx2-GFP
Recombinant DNA reagent	pActin-Gal4	DGRC		Actin promoter Gal4 for insect UAS expression
Recombinant DNA reagent	pCMV-Gal4	Addgene	#24345	CMV promoter Gal4 for mammalian UAS expression
Antibody	Anti-Atx2 (chicken polyclonal)	Bakthavachalu et al., 2018	N/A	IF (1:1000) WB (1:1000)
Antibody	Anti-Caprin (rabbit polyclonal)	Papoulas et al., 2010	N/A	IF (1:1000)
Antibody	Anti-dFMR (mouse monoclonal)	DSHB	# 5A11	IF (1:1000) deposited to the DSHB by Siomi, H.
Antibody	Anti-GFP (chicken polyclonal)	Abcam	Cat# mAb 13970	IF (1:1000)
Antibody	Anti-V5 (rabbit polyclonal)	Santa Cruz Biotechnology	Cat# sc83849-R	IF (1:1000) WB (1:1000)
Antibody	PABP (rabbit polyclonal serum)	Lee et al. 2017	N/A	IF (1:500) WB (1:500)
Antibody	Me31B (rabbit polyclonal serum)	Lee et al. 2018	N/A	IF (1:500)
Antibody	Rox8 (rat polyclonal)	Buddika et al. 2020	N/A	IF (1:1000)
Antibody	SNAP (rabbit polyclonal)	NEB	Cat# P9310S	WB (1:1000)
Antibody	PABPC1 (rabbit polyclonal)	Abcam	Cat# ab21060	WB (1:1000)
Antibody	LSM12 (rabbit anti human polyclonal)	Abcam	Cat# ab173292	WB (1:1000)
Antibody	G3BP (mouse monoclonal)	BD Bioscience	Cat# 611126	IF (1:1000)
Antibody	Histone H3 (rabbit polyclonal)	Cell signaling tech	Cat# 9715	WB (1:1000)
Antibody	Baf155 (rabbit monoclonal)	Cell signaling tech	Cat# 11956	WB (1:1000)

Antibody	HRP Goat anti-rabbit	Invitrogen	Cat# A16104	WB (1:10,000)
Antibody	HRP Goat anti-mouse	Invitrogen	Cat# 31430	WB (1:10,000)
Antibody	Alexa Fluor 555 (polyclonal goat anti-chicken IgG)	Invitrogen	Cat# A21437	IF (1:1000)
Antibody	Alexa Fluor 488 (polyclonal goat anti-chicken IgG)	Invitrogen	Cat# A11039	IF (1:1000)
Antibody	Alexa Fluor 647 (polyclonal goat anti-chicken IgG)	Invitrogen	Cat# A21449	IF (1:1000)
Antibody	Alexa Fluor 555 (polyclonal goat anti-rabbit IgG)	Invitrogen	Cat# A21428	IF (1:1000)
Antibody	Alexa Fluor 488 (polyclonal goat anti-rabbit IgG)	Invitrogen	Cat# A11078	IF (1:1000)
Antibody	Alexa Fluor 647 (polyclonal goat anti-rabbit IgG)	Invitrogen	Cat# A21244	IF (1:1000)
Antibody	Alexa Fluor 555 (polyclonal goat anti-mouse IgG)	Invitrogen	Cat# A21422	IF (1:1000)
Antibody	Alexa Fluor 488 (polyclonal goat anti-mouse IgG)	Invitrogen	Cat# A21121	IF (1:1000)
Antibody	Alexa Fluor 647 (polyclonal goat anti-mouse IgG)	Invitrogen	Cat# A21235	IF (1:1000)
Chemical compound	MOWIOL mounting medium	Sigma (Merck)	Cat# 81381	
Chemical compound	SNAP-TmrStar	New England Biolabs	Cat# S9105S	IF (1:1000)
Chemical compound	SNAP-Surface 488	New England Biolabs	Cat# S9124S	IF (1:1000)
Software, algorithm	TRIBE	McMahon et al., 2016	https://github.com/rosbashlab/TRIBE	
Software, algorithm	STAR v2.5.3	Dobin et al., 2013	https://github.com/alexdobin/STAR	
Software, algorithm	HTSeq v0.11.2	Anders et al., 2015	https://github.com/htseq/htseq	
Software, algorithm	DESeq2	Love et al., 2014	https://bioconductor.org/packages/release/bioc/html/DESeq2.html	
Software, algorithm	ARE*Score*	Spasic et al., 2012	http://arescore.dkfz.de/arescore.pl	
Software, algorithm	Guitar	Cui et al., 2016	https://bioconductor.org/packages/release/bioc/html/Guitar.html	
Software, algorithm	Bedtools	Quinlan and Hall, 2010	https://github.com/arq5x/bedtools2	
Software, algorithm	twoBitToFa	-	https://genome.ucsc.edu/goldenPath/help/twoBit.html	
Software, algorithm	MEME suite	Bailey et al., 2009	http://meme-suite.org/tools/meme	
Software, algorithm	ImageJ	Schneider et al., 2012	https://imagej.nih.gov/ij/	

Software, algorithm	Ggplot2	Wilkinson, 2011	https://github.com/tidyverse/ggplot2	
Software, algorithm	Pheatmap		https://cran.r-project.org/web/packages/pheatmap/index.html	
Software, algorithm	SnapDragon		https://www.flyrnai.org/snapdragon	

564

565 Cell culture, transfection and stress induction

566 *Drosophila* S2R+ cells were obtained from the DGRC, Indiana University, and were grown in
567 Gibco Schneider's S2 media with 10% FBS and 1% penicillin and streptomycin, at 25°C.
568 Transfections were performed using either FugeneHD (Active Motif) or TransIT-X2 (Mirus)
569 reagents at 2:1 ratio µl reagent to µg plasmid DNA for 24-72 h depending on downstream use.
570 HEK293T cells from Adrian Bracken, Trinity College Dublin, were grown in Gibco
571 Dulbecco's Modified Eagle Media with 10% FBS, 2 mM l-glutamine addition, 1% penicillin
572 and streptomycin, at 37°C and 5% CO2. U2OS cells from Martina Schroeder, Maynooth
573 University, were grown at the same conditions as HEK293T. Mammalian cell transfections
574 were carried out with 1 mM PEI (Polysciences) solution at 2:1 ratio µl reagent to µg plasmid
575 DNA for 24-72H depending on downstream use. For confocal imaging applications cells were
576 grown in 24-well plates on glass cover-slips for 24 h before transfection for up to 48 h. For
577 Western blotting and IP, cells were grown in 75 cm^2 flasks until >80% confluent before
578 transfection for up to 72H before harvesting. Oxidative stress was induced in *Drosophila* S2R+
579 cells with addition of sodium arsenite solution to a final concentration of 50 µM in media for
580 3 h. In mammalian cells, oxidative stress was induced in the same way except for only 1 h.

581

582 Western blotting and protein immunoprecipitation

583 Total protein extracts were prepared from S2 and HEK293 cells as described earlier
584 (Sudhakaran et al., 2014). Up to 10 µg total protein was loaded per well for detecting Atx2-
585 SNAP constructs, partner proteins and loading controls on 8-12% SDS-PAGE gels and
586 transferred to nitrocellulose membranes. The blots were probed in 5% skim milk in PBS using
587 rabbit anti-SNAP (1:1000), rabbit anti-PABP (1:1000), rabbit anti-LSM12 (1:1000) antibodies,
588 and mouse anti-histone H3 (1:5000) and mouse anti-BAF155 (1:2000) loading control
589 antibodies. Corresponding HRP-conjugated secondary antibodies were used at 1:10,000
590 dilution and developed using Pierce ECL western blotting substrate (ThermoFisher) as per the
591 manufacturer's instructions.

For Atx2-SNAP construct immunoprecipitation, transfected cell lysates were normalised to the same volume and concentration, 10% of the volume was saved and diluted as an input control, and Chromotek anti-SNAP-tag conjugated agarose beads and IP kits were used according to the manufacturer's specifications. Pulled-down proteins together with corresponding sample input controls were blotted as described above.

Immunohistochemistry and imaging of cultured cells

Transfected cells on coverslips were fixed with 4% paraformaldehyde in PBS solution for 15 min, followed by three 5 min washes in PBS. Permeabilization was performed on all cells with 0.5% TritonX100 in PBS solution for 3 min, before three more 5 min washes in PBS. Cells were blocked with 3% BSA in PBS for 1 h at room temperature before staining with primary antibodies at appropriate dilutions in 3% BSA overnight at 4°C. Corresponding fluorescent secondary antibodies in 3% BSA were used to stain the sample cells for 1 h at room temperature after primaries were washed off. Where SNAP-tagged proteins were being visualized, SNAP-ligand TMR-Star (NEB) or SNAP-surface-Alexa488 (NEB) were added at the secondary antibody staining stage. Following staining and washing, cells were mounted upside-down on microscopy slides in MOWIOL, allowed to cure for >12 h at 4 °C, and imaged on a Zeiss LSM880 Airyscan/AiryscanFast confocal microscope with a 20x air objective.

Bioimage analysis

Where relevant, Airyscan images were processed with Zen Black software (Zeiss) with recommended settings. Confocal microscopy images were analysed using macros within ImageJ/FIJI and Excel. Quantification of co-localisation was performed by comparing stress granule marker staining intensity profiles across a randomised selection of Atx2 granules within transfected cells, with the intensity profile of the Atx2 staining. Any signal 10% or higher than background (adjusted for fluorophore bleed through) was deemed evidence of co-localisation within that particular granule. For quantifying the exclusion of mini-Atx2-SNAP constructs from stress induced granules the Caprin or G3BP1 staining was used as independent identifier of stress granules and Atx2 profiles were compared to them. 48-120 granules were quantified in each co-staining (Figure 2), and 28-70 granules were quantified for each construct transfection (Figure 4).

Crystal structure threading

Threading of the *Drosophila* PAM2 peptide bound to the MLLE domain of PABPC1 was performed using the Swiss-PdbViewer software, based on the human crystal structure of the complex obtained from PDB, identified as 3KTR (Kozlov et al., 2010)

Experimental fly crosses

Drosophila stocks were maintained at 25°C in corn meal agar. Strains homozygous for UAS-transgenes were crossed with *elav-Gal4* and *tub-Gal80ts* at 18 °C till the adult fly emerged. The flies were shifted to 29 °C for 5 days before processing for RNA extraction for TRIBE experiments. The climbing behaviour experiments were performed on flies kept at 29 °C for either 1 or 15 days. For microCT experiments, the UAS-transgenes were crossed with *mef2-Gal4* and *tub-Gal80ts* at 18°C and the adult flies were transferred to 29 °C for 1 day or 20 days.

RNA extraction from brain and NGS

Around 10-12 adult brains were dissected in RNA Later for total RNA isolation. RNA was isolated using TRIzol reagent (Invitrogen) as per the manufacturer's protocol. Poly(A)-enriched mRNA was used to prepare Illumina libraries using the NEBNext Ultra II Directional RNA Library Prep kit (E7765L). Atx2-ΔPAM2-ADARcd samples were sequenced with Illumina HiSeq PE Rapid Cluster Kit v2 (PE-402-4002) to generate 2 × 100 paired-end strand-specific data using the Illumina HiSeq 2500 sequencing platform.

TRIBE data analysis

The sequencing reads obtained had a mean quality score (Q-Score) >= 37. Analysis of the TRIBE data was performed as described previously (McMahon et al., 2016, Singh et al., 2021). Briefly, the reference genome and gtf file of *Drosophila melanogaster*, version dm6, were downloaded from the UCSC genome browser. Raw sequencing reads were mapped using TopHat2 (Trapnell *et al*, 2009) with the parameters '--library-type fr-firststrand -m 1 N 3 --read-edit-dist 3 p 5 g 2 -I 50000 --microexon-search --no-coverage-search -G dm6_genes.gtf'. Only uniquely mapped reads are considered for editing analysis. A table of raw and mapped reads is included in Supplementary Table 1. A threshold file was created by ensuring only edits with coverage of at least 20 reads and 15% edits were retained. All the TRIBE experiments were performed in duplicates, and only the edits identified in both replicates above the edit threshold are reported.

Climbing Assay:

Appropriately aged adult *Drosophila* was transferred to a 50 ml graduated glass measuring cylinder for the climbing assay and sealed with a cotton plug. A digital video camera was positioned to record the vials. The assay was initiated by tapping the cylinder against a foam pad to collect the flies to the bottom of the cylinder and the flies were allowed to climb the cylinder with video being recorded for ~30 s. The number of flies that crossed the 20 ml mark (~5.5cm) was counted over time and the data was plotted against the time using GraphPad prism. Average of 3 trials were used for each biological replicate. 7-10 biological replicates were used for each genotype.

Sample preparation and scanning for microCT**:**

Drosophila indirect flight muscle microCT was carried out as described in Chaturvedi et. al, 2019. Briefly, animals were anesthetized on ice and fixed in PBS containing 4% paraformaldehyde (PFA). Thoraces were dissected and stained using 1% elemental iodine (1.93900.0121, Emparta, Merck) with 2% potassium iodide (no. 15 724, Qualigens) dissolved in PBS. The stained samples were washed in PBS and embedded in petroleum jelly. MicroCT scanning was carried out at 40 kV, 250 µA, on Bruker Skyscan-1272.

Data availability

The RNA sequencing data have been deposited to GEO under the accession code GSE196739.

Contact for reagent and resource sharing

Further information and requests for resources and reagents should be directed to and will be fulfilled by the lead contacts Mani Ramaswami (mani.ramaswami@tcd.ie) and Baskar Bakthavachalu (baskar@iitmandi.ac.in).

ACKNOWLEDGEMENTS:

We thank members of the Ramaswami, Vijay Raghavan and Bakthavachalu labs and Roy Parker for useful discussions and/or comments on the manuscript. We thank Marlena Mucha, Adrian Bracken and Amir Khan for advice and help with biochemical experiments, Michael Rosbash for *Drosophila* TRIBE plasmids, and colleagues acknowledged in the Key Resources table for reagents and advice. The fly facility at Bangalore Life Science Cluster (BLiSC)

provided support with fly stock supply as well as generation of transgenic; CIFF at BLiSC provided essential confocal microscopy support; and Awadhesh Pandit and next-generation genomics facility at BLiSC provided NGS service. Daniel Fortunati thanks Kenneth Mok for his mentorship. We acknowledge Drosophila Genomics Resource Centre (supported by NIH grant 2P40OC010949) for *Drosophila* S2 cells.

FUNDING:

The work was supported by a Science Foundation Ireland (SFI) Investigator grant to MR and NCBS-TIFR intramural funding to KVR. BB is supported by the DBT/Wellcome Trust India Alliance Fellowship (IA/I/19/1/504286). We acknowledge the support from an Irish Research Council Postgraduate Fellowship to DF, the J. C. Bose Fellowship of the Government of India (KVR), INSA Young Scientist Project (INSA/SP/YSP/143/2017) (AS), SERB to MR from a collaborative VAJRA award to Dr. Raghu Padinjat, and a DST INSPIRE fellowship (KA). We thank C-CAMP for logistical support for SSP.

AUTHOR CONTRIBUTIONS:

Conceptualization, A.P., D.F, A.S., J.Huelsmeier, K.V.R., M.R., and B.B.; Methodology, A.P., D.F, A.S., J.Huelsmeier, A.R.K., S.S.P., J.Hillebrand, K.A., D.J., G.B., J.L., C.L., G.A., K.H.M., K.V.R., M.R., and B.B.; Investigation, A.S., J.Huelsmeier, A.R.K., S.S.P., J.Hillebrand, A.P., K.A., K.V.R., M.R., and B.B.; Writing–Original Draft, A.P., D.F, A.S., J.Huelsmeier, K.V.R., M.R., and B.B.; Writing–Review & Editing, A.P., D.F, A.S., J.Huelsmeier, A.R.K., S.S.P., J.Hillebrand, K.A., D.J., G.B., J.L., C.L., G.A., K.H.M., K.V.R., M.R., and B.B.; Funding Acquisition, K.V.R., M.R., and B.B.; Resources, Fly community.

DECLARATION OF INTERESTS: The authors declare no conflicts of interest.

SUPPLEMENTARY FIGURES:

Supplementary Figure 1:

A.

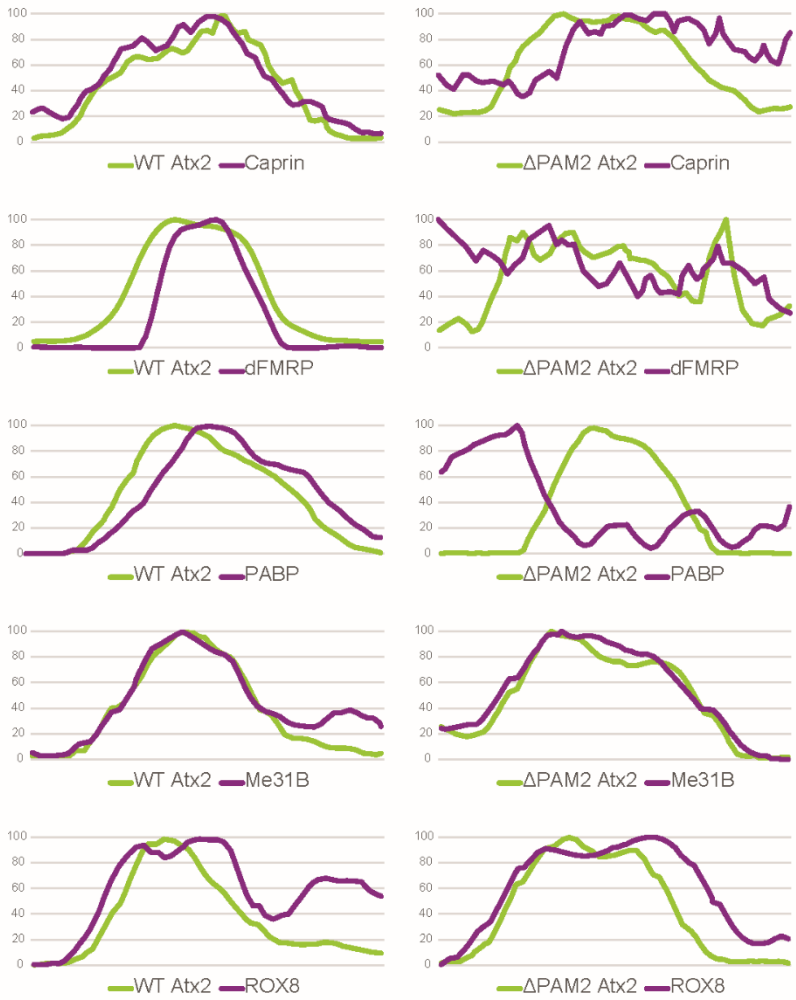

B.

Co-localisation of signal enrichment in granules		
	WT Atx2	ΔPAM2 Atx2
Caprin	100.0%	7.1%
dFMRP	100.0%	2.4%
PABP	76.7%	14.6%
Me31B	66.7%	52.0%
Rox8	100%	100%

C.

	Drosophila Mini Atx2-SNAP Version						
Construct	WT	ΔLSm	ΔLSm-AD	ΔPAM2	L859A	F866A	Double*
% enrichment in SGs	88.60%	80.00%	93.30%	4.60%	0.00%	0.00%	0.00%
	Human Mini Atxn2-SNAP Version						
Construct	WT	ΔLSm	ΔLSm-AD	ΔPAM2	L914A	F921A	Triple*
% enrichment in SGs	100.00%	96.20%	100.00%	4.90%	0.00%	5.00%	4.80%

Supplementary Figure 1: Co-localisation quantification for figure 2, figure 4. (A) Normalised profile plots of Atx2-GFP granules in S2 cells as shown in Figure 2. Within representative granules of wild type Atx2-GFP (green line), SG components Caprin, dFMRP, PABP, Me31B, and Rox8 show largely overlapping enrichment of fluorescence profile along a line bisecting a granule after immunohistochemistry and imaging (purple line). In Atx2ΔPAM2-GFP granules,

this colocalization of fluorescence signals is not seen in the case of Caprin, dFMRP and PABP, suggesting these components are not enriched in these granules above background level. (B) Quantification of co-localization for Figure 2. N = 48-120 images of Atx2-GFP granules were randomly selected for each co-staining and analysed for signal co-enrichment (see methods) in the case of each component assayed. (C) Quantification of Atx2 construct inclusion in SGs for Figure 4. N = 28-70 images of stress granules in arsenite stressed S2 cells (marked by anti-Caprin staining) and U2OS cells (marked by anti-G3BP staining) were randomly selected for each Atx2 construct assayed and were analysed for Mini Atx2-SNAP allele signal co-enrichment (see methods).

737 **Supplementary Figure 2:**

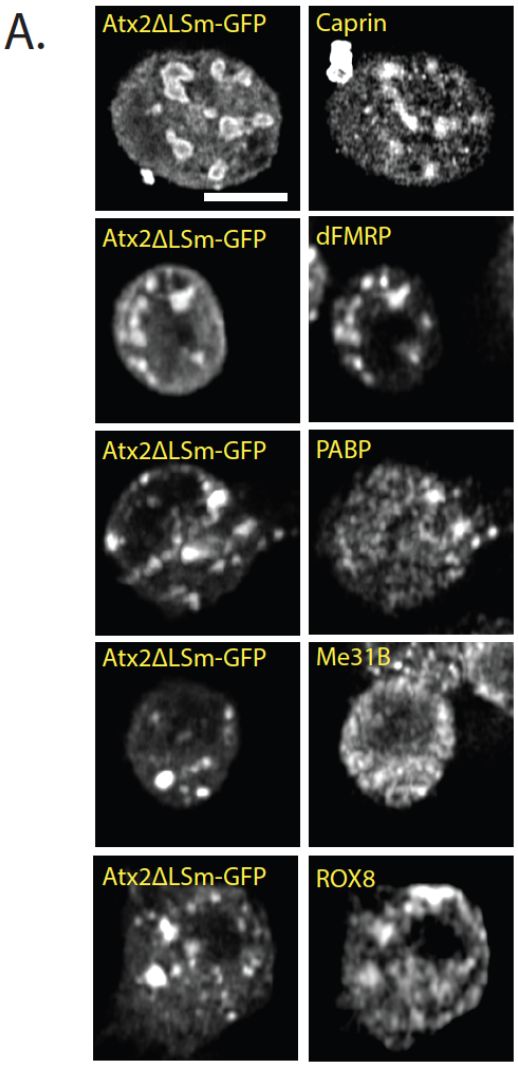

738

739 **Supplementary Figure 2:** Atx2ΔLSm granules in S2 cells do not show significantly altered
740 protein contents compared to wild-type Atx2. Caprin, dFMRP, PABP, Me31B, and Rox8 co-
741 localize with overexpressed Atx2ΔLSm GFP, suggesting that the granules formed contain a
742 similar set of components as Atx2 granules. It should be noted that Atx2 granules do not
743 sequester the majority of the endogenous components stained for, leading to a high, diffuse
744 background staining.

745

746 **Supplementary Figure 3:**

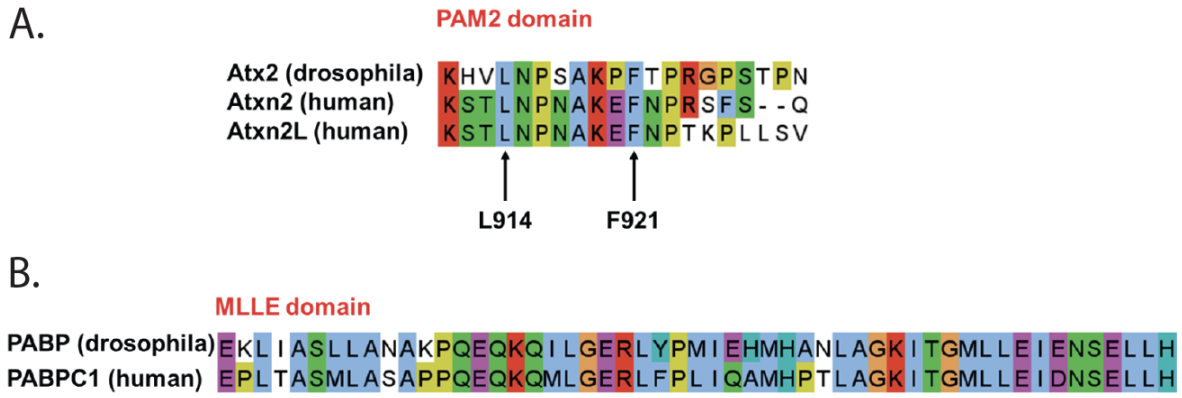

747

748

749 **Supplementary Figure 3:** The ATXN2 PAM2 and the PABPC1 MLLE domain are highly
750 conserved from fly to human. (A) The ATXN2 PAM2 domain exhibits high sequence
751 similarity where the key MLLE domain hydrophobic binding residues leucine 914 and
752 phenylalanine 921 (human ATXN2 numbering) are conserved from *Drosophila* to humans. (B)
753 Its binding partner, the PABPC1 MLLE domain, is also highly conserved from *Drosophila* to
754 human. Sequence IDs: Q8SWR8 (Atx2_DROME), Q99700 (ATXN2_HUMAN), Q8WWM7
755 (ATX2L_HUMAN), P21187 (PABP_DROME), P11940 (PABP1_HUMAN).

756

757

Supplementary Figure 4:

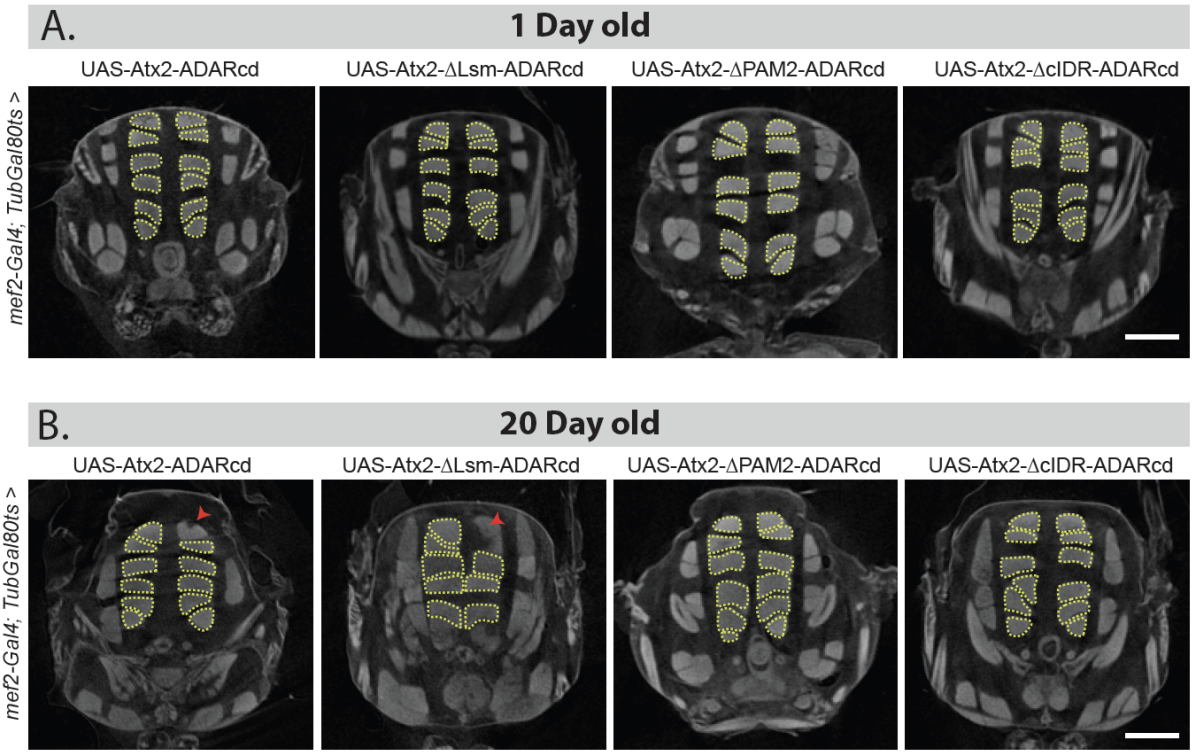

Supplementary Figure 4: Transverse view of *Drosophila* indirect flight muscle imaged using micro-CT show cellular toxicity. (A) Driving UAS-transgene (Atx2WT, Atx2ΔcIDR, Atx2ΔPAM or Atx2ΔLSm) with *mef2-Gal4* show normal muscles on day 1. (B) Expression of wild-type and Atx2ΔLSm transgene for 20 days show loss of muscle fibers, indicated with solid red arrowheads. Expression of Atx2ΔPAM2 and Atx2ΔcIDR for 20 days show no visible phenotype.

Supplementary Table 1:

S.NO	Sample Name	Million reads (Paired end)		Total Number of Million reads	% >= Q30	Mean Quality Score	Mapping Percentage Read 1	Mapping Percentage Read 2
		Read 1	Read 2					
1	Atx2ΔPAM2-ADARcd rep_1	23.75	23.75	47	97.04	38.26	92.20%	92.10%
2	Atx2ΔPAM2-ADARcd rep_2	22.66	22.66	45	97.03	38.26	91.30%	91.20%

Supplementary Table 2: The targets common between Atx2 wild-type and del-PAM2 are shown in bold text.

Chr	Start	End	Genes	Replicate 1 edit percentage	Replicate 2 edit percentage	Average edit percentage	Chr_coordinate
chr2L	**1009080**	**1009081**	**IA-2**	**17.1**	**15.5**	**16.3**	**chr2L_1009081_IA-2**
chr2L	**1009440**	**1009441**	**IA-2**	**31.7**	**38.8**	**35.25**	**chr2L_1009441_IA-2**
chr2L	**1011482**	**1011483**	**IA-2**	**31.7**	**34.7**	**33.2**	**chr2L_1011483_IA-2**
chr2L	13505104	13505105	B4	22.4	17.48	19.94	chr2L_13505105_B4
chr2L	**17188307**	**17188308**	**beat-IIIc**	**18**	**21.7**	**19.85**	**chr2L_17188308_beat-IIIc**
chr2L	19746161	19746162	CG10631	25.65	19.4	22.52	chr2L_19746162_CG10631
chr2L	**20056018**	**20056019**	**sNPF**	**16**	**24.3**	**20.15**	**chr2L_20056019_sNPF**
chr2L	7891375	7891376	Snoo	18.5	16.7	17.6	chr2L_7891376_Snoo
chr2L	8113160	8113161	Bsg	17.4	19.05	18.23	chr2L_8113161_Bsg
chr2L	**8113894**	**8113895**	**Bsg**	**16.82**	**28.7**	**22.76**	**chr2L_8113895_Bsg**
chr2L	8116005	8116006	Bsg	18.2	27.4	22.8	chr2L_8116006_Bsg
chr2L	9256901	9256902	Ggamma30A	19.5	32.6	26.05	chr2L_9256902_Ggamma30A
chr2L	**9292530**	**9292531**	**Ggamma30A**	**42**	**54.4**	**48.2**	**chr2L_9292531_Ggamma30A**
chr2L	**9292829**	**9292830**	**Ggamma30A**	**42.6**	**53.55**	**48.08**	**chr2L_9292830_Ggamma30A**
chr2L	9295031	9295032	Ggamma30A	23.5	26	24.75	chr2L_9295032_Ggamma30A
chr2R	12085463	12085464	jeb	16	28.4	22.2	chr2R_12085464_jeb
chr2R	**13513577**	**13513578**	**Vmat**	**64.2**	**63.9**	**64.05**	**chr2R_13513578_Vmat**
chr2R	13513654	13513655	Vmat	27.7	33.45	30.58	chr2R_13513655_Vmat
chr2R	**13513732**	**13513733**	**Vmat**	**24**	**29.75**	**26.88**	**chr2R_13513733_Vmat**
chr2R	**13513762**	**13513763**	**Vmat**	**44.55**	**47.3**	**45.92**	**chr2R_13513763_Vmat**
chr2R	**13514350**	**13514351**	**Vmat**	**37.7**	**38.5**	**38.1**	**chr2R_13514351_Vmat**
chr2R	13519080	13519081	Vmat	18.1	20.8	19.45	chr2R_13519081_Vmat
chr2R	**23690701**	**23690702**	**Pal2**	**17.3**	**17.2**	**17.25**	**chr2R_23690702_Pal2**
chr2R	24213943	24213944	CG30419	27.8	22.98	25.39	chr2R_24213944_CG30419
chr2R	24214234	24214235	CG30419	24.2	26.1	25.15	chr2R_24214235_CG30419
chr2R	24214648	24214649	CG30419	16.4	15.9	16.15	chr2R_24214649_CG30419
chr2R	24215193	24215194	CG30419	43.5	29.7	36.6	chr2R_24215194_CG30419
chr2R	24229341	24229342	CG30419	20.8	16.3	18.55	chr2R_24229342_CG30419
chr2R	6914804	6914805	CG30158	16.4	16	16.2	chr2R_6914805_CG30158
chr2R	**6920815**	**6920816**	**CG30158**	**33.92**	**40.48**	**37.2**	**chr2R_6920816_CG30158**
chr2R	**6921435**	**6921436**	**CG30158**	**17.5**	**41.9**	**29.7**	**chr2R_6921436_CG30158**
chr2R	**6921976**	**6921977**	**CG30158**	**36**	**40.2**	**38.1**	**chr2R_6921977_CG30158**
chr2R	**7718070**	**7718071**	**CG18812**	**15.9**	**19.7**	**17.8**	**chr2R_7718071_CG18812**

chr2R	9473772	9473773	Camta	21.75	30.18	25.96	chr2R_9473773_Camta
chr2R	9479421	9479422	Camta	23.1	26	24.55	chr2R_9479422_Camta
chr2R	**9480019**	**9480020**	**Camta**	**32**	**41**	**36.5**	**chr2R_9480020_Camta**
chr2R	**9910328**	**9910329**	**FMRFa**	**42.5**	**25**	**33.75**	**chr2R_9910329_FMRFa**
chr3L	**11498209**	**11498210**	**chrb**	**15.82**	**20.5**	**18.16**	**chr3L_11498210_chrb**
chr3L	12267895	12267896	CG32100	20	16.1	18.05	chr3L_12267896_CG32100
chr3L	1504295	1504296	Psa	18.6	15.9	17.25	chr3L_1504296_Psa
chr3L	1521650	1521651	Psa	18.5	34.6	26.55	chr3L_1521651_Psa
chr3L	1543675	1543676	CG7852	15.5	22	18.75	chr3L_1543676_CG7852
chr3L	17062355	17062356	Rbp6	15.2	18.5	16.85	chr3L_17062356_Rbp6
chr3L	17147382	17147383	Rbp6	18.23	26.62	22.42	chr3L_17147383_Rbp6
chr3L	**17345219**	**17345220**	**Mip**	**29.9**	**27.2**	**28.55**	**chr3L_17345220_Mip**
chr3L	**17345290**	**17345291**	**Mip**	**17.9**	**16.9**	**17.4**	**chr3L_17345291_Mip**
chr3L	**19066983**	**19066984**	**Mkp3**	**18.9**	**15.7**	**17.3**	**chr3L_19066984_Mkp3**
chr3L	21494821	21494822	Hr78	27.1	18.4	22.75	chr3L_21494822_Hr78
chr3L	21831417	21831418	CG7148	15.8	28.6	22.2	chr3L_21831418_CG7148
chr3L	21930851	21930852	mub	15	17.2	16.1	chr3L_21930852_mub
chr3L	21931110	21931111	mub	15.1	20.1	17.6	chr3L_21931111_mub
chr3L	22061206	22061207	Oct-TyrR	15.4	16.7	16.05	chr3L_22061207_Oct-TyrR
chr3L	22877661	22877662	Chro	35.3	45.7	40.5	chr3L_22877662_Chro
chr3L	23148124	23148125	CG32350	27.4	35.3	31.35	chr3L_23148125_CG32350
chr3L	23747549	23747550	CG17698	40.27	28.95	34.61	chr3L_23747550_CG17698
chr3L	23934990	23934991	CG40470	23.5	22.05	22.77	chr3L_23934991_CG40470
chr3L	3910071	3910072	Eip63F-1	20	24.5	22.25	chr3L_3910072_Eip63F-1
chr3L	**3954338**	**3954339**	**CG12605**	**35.2**	**40.8**	**38**	**chr3L_3954339_CG12605**
chr3L	**3954933**	**3954934**	**CG12605**	**35.42**	**51.1**	**43.26**	**chr3L_3954934_CG12605**
chr3L	3957068	3957069	CG12605	21.8	26.7	24.25	chr3L_3957069_CG12605
chr3L	3957671	3957672	CG12605	18.9	22.2	20.55	chr3L_3957672_CG12605
chr3L	3961590	3961591	CG12605	18.3	18.5	18.4	chr3L_3961591_CG12605
chr3L	3992789	3992790	scrt	21.08	27.28	24.18	chr3L_3992790_scrt
chr3L	4092142	4092143	CG14989	15.88	18.6	17.24	chr3L_4092143_CG14989
chr3L	4113123	4113124	Ack	18.4	16.7	17.55	chr3L_4113124_Ack
chr3L	4113297	4113298	Ack	18.4	17.9	18.15	chr3L_4113298_Ack
chr3L	572527	572528	hipk	29.8	31	30.4	chr3L_572528_hipk
chr3L	572530	572531	hipk	42.7	43	42.85	chr3L_572531_hipk
chr3L	**575712**	**575713**	**hipk**	**36.12**	**52.92**	**44.52**	**chr3L_575713_hipk**
chr3L	**575753**	**575754**	**hipk**	**31.7**	**49.6**	**40.65**	**chr3L_575754_hipk**
chr3L	576730	576731	hipk	17.1	15.2	16.15	chr3L_576731_hipk
chr3L	577020	577021	hipk	20	16.9	18.45	chr3L_577021_hipk
chr3L	**577417**	**577418**	**hipk**	**51.42**	**62.12**	**56.77**	**chr3L_577418_hipk**
chr3L	577970	577971	hipk	21.4	25.9	23.65	chr3L_577971_hipk
chr3L	578186	578187	hipk	18.2	24.9	21.55	chr3L_578187_hipk
chr3L	578453	578454	hipk	25.7	32.7	29.2	chr3L_578454_hipk
chr3L	579335	579336	hipk	18.1	17	17.55	chr3L_579336_hipk
chr3L	579634	579635	hipk	20.5	19.8	20.15	chr3L_579635_hipk

chr3L	**580103**	**580104**	**hipk**	**63.1**	**67.7**	**65.4**	**chr3L_580104_hipk**
chr3L	580500	580501	hipk	15.6	18.1	16.85	chr3L_580501_hipk
chr3L	580932	580933	hipk	17.9	24.1	21	chr3L_580933_hipk
chr3L	**8970787**	**8970788**	**CG5026**	**17.9**	**16.7**	**17.3**	**chr3L_8970788_CG5026**
chr3L	8993382	8993383	smg	25.9	15.3	20.6	chr3L_8993383_smg
chr3L	9074752	9074753	Tequila	29.8	19.5	24.65	chr3L_9074753_Tequila
chr3L	**9103274**	**9103275**	**bol**	**23.9**	**26.3**	**25.1**	**chr3L_9103275_bol**
chr3L	9136454	9136455	Use1	25	16	20.5	chr3L_9136455_Use1
chr3L	9669496	9669497	fry	18.2	18.2	18.2	chr3L_9669497_fry
chr3L	9945905	9945906	CG34356	19.4	32.1	25.75	chr3L_9945906_CG34356
chr3R	10158991	10158992	Invadolysin	17.9	18.2	18.05	chr3R_10158992_Invadolysin
chr3R	10862820	10862821	CG6574	20.8	33.3	27.05	chr3R_10862821_CG6574
chr3R	10877257	10877258	CR45195	32.7	19.5	26.1	chr3R_10877258_CR45195
chr3R	10889941	10889942	Leash	18.2	18.8	18.5	chr3R_10889942_Leash
chr3R	**13224637**	**13224638**	**Ace**	**24.8**	**33.3**	**29.05**	**chr3R_13224638_Ace**
chr3R	**13227870**	**13227871**	**Ace**	**26.6**	**35.3**	**30.95**	**chr3R_13227871_Ace**
chr3R	**13227970**	**13227971**	**Ace**	**33.42**	**47.95**	**40.69**	**chr3R_13227971_Ace**
chr3R	14330745	14330746	NK7.1	16.2	16.7	16.45	chr3R_14330746_NK7.1
chr3R	14660839	14660840	Hexim	17.1	20	18.55	chr3R_14660840_Hexim
chr3R	14669984	14669985	Meltrin	16.95	20.7	18.82	chr3R_14669985_Meltrin
chr3R	14746335	14746336	jvl	36.4	20.9	28.65	chr3R_14746336_jvl
chr3R	14746546	14746547	smp-30	45.1	24	34.55	chr3R_14746547_smp-30
chr3R	**14804349**	**14804350**	**btsz**	**16.5**	**26.5**	**21.5**	**chr3R_14804350_btsz**
chr3R	**15255687**	**15255688**	**CG42404**	**18.2**	**17.6**	**17.9**	**chr3R_15255688_CG42404**
chr3R	15356475	15356476	Atg4b	15.4	20.7	18.05	chr3R_15356476_Atg4b
chr3R	15414730	15414731	Atx2	22.82	26.25	24.54	chr3R_15414731_Atx2
chr3R	15414731	15414732	Atx2	19	22.6	20.8	chr3R_15414732_Atx2
chr3R	15849417	15849418	cv-d	18.8	22.2	20.5	chr3R_15849418_cv-d
chr3R	**16611267**	**16611268**	**NPF**	**22.98**	**23.52**	**23.25**	**chr3R_16611268_NPF**
chr3R	16645743	16645744	CG10324	26.1	35	30.55	chr3R_16645744_CG10324
chr3R	17090737	17090738	cal1	25	15.4	20.2	chr3R_17090738_cal1
chr3R	**17731884**	**17731885**	**Lgr1**	**20**	**19**	**19.5**	**chr3R_17731885_Lgr1**
chr3R	17802763	17802764	CG17806	20.7	18.8	19.75	chr3R_17802764_CG17806
chr3R	19155252	19155253	CG11779	15.6	19.1	17.35	chr3R_19155253_CG11779
chr3R	20783186	20783187	Syp	21.1	17	19.05	chr3R_20783187_Syp
chr3R	20797469	20797470	Syp	15.3	20	17.65	chr3R_20797470_Syp
chr3R	20820785	20820786	CG17271	31.2	19.75	25.48	chr3R_20820786_CG17271
chr3R	20862212	20862213	CG3822	17	26.3	21.65	chr3R_20862213_CG3822
chr3R	20992668	20992669	Calx	17.8	27.5	22.65	chr3R_20992669_Calx
chr3R	21213891	21213892	SNF4Agamma	17.2	20	18.6	chr3R_21213892_SNF4Agamma
chr3R	21354284	21354285	mod(mdg4)	15	19	17	chr3R_21354285_mod(mdg4)
chr3R	21527750	21527751	CG7956	30.3	26.5	28.4	chr3R_21527751_CG7956
chr3R	21625731	21625732	E2f	18	23.7	20.85	chr3R_21625732_E2f
chr3R	23261698	23261699	orb	15.2	16.1	15.65	chr3R_23261699_orb

chr3R	23681818	23681819	eIF-3p66	20.4	21.5	20.95	chr3R_23681819_eIF-3p66
chr3R	**23698883**	**23698884**	**prt**	**15.4**	**23.4**	**19.4**	**chr3R_23698884_prt**
chr3R	23723418	23723419	CG10365	16.1	21.1	18.6	chr3R_23723419_CG10365
chr3R	23732353	23732354	Rpn9	20.4	16.7	18.55	chr3R_23732354_Rpn9
chr3R	24664388	24664389	slo	23.1	30	26.55	chr3R_24664389_slo
chr3R	24802164	24802165	polybromo	29.2	20.98	25.09	chr3R_24802165_polybromo
chr3R	24820485	24820486	Saf-B	15	22	18.5	chr3R_24820486_Saf-B
chr3R	25234647	25234648	CG10420	22.2	34.5	28.35	chr3R_25234648_CG10420
chr3R	**26233920**	**26233921**	**CG12290**	**25.6**	**18.4**	**22**	**chr3R_26233921_CG12290**
chr3R	**28050111**	**28050112**	**CG34362**	**15.6**	**25.6**	**20.6**	**chr3R_28050112_CG34362**
chr3R	28838531	28838532	Apc	20.4	18.8	19.6	chr3R_28838532_Apc
chr3R	29659085	29659086	Dop1R2	15.8	39.5	27.65	chr3R_29659086_Dop1R2
chr3R	**29674515**	**29674516**	**Bub3**	**27.6**	**17.8**	**22.7**	**chr3R_29674516_Bub3**
chr3R	31457698	31457699	Gprk2	23.5	24.5	24	chr3R_31457699_Gprk2
chr3R	31841367	31841368	RhoGAP100F	17.73	19	18.37	chr3R_31841368_RhoGAP100F
chr3R	**5811503**	**5811504**	**CG11000**	**21.3**	**32.4**	**26.85**	**chr3R_5811504_CG11000**
chr3R	**5811505**	**5811506**	**CG11000**	**20.8**	**25.7**	**23.25**	**chr3R_5811506_CG11000**
chr3R	7126383	7126384	CG10098	18.6	19.1	18.85	chr3R_7126384_CG10098
chr3R	8244435	8244436	CG18749	15.4	16.1	15.75	chr3R_8244436_CG18749
chr3R	8244435	8244436	CG33722	15.4	16.1	15.75	chr3R_8244436_CG33722
chr3R	9416762	9416763	alpha-Man-II	30.8	32.3	31.55	chr3R_9416763_alpha-Man-II
chr3R	9441505	9441506	ps	37.92	33.52	35.72	chr3R_9441506_ps
chr3R	9471135	9471136	CG16779	43.05	34.85	38.95	chr3R_9471136_CG16779
chr3R	9525979	9525980	CG8176	16.2	24.4	20.3	chr3R_9525980_CG8176
chr3R	9539464	9539465	mura	21.75	20.05	20.9	chr3R_9539465_mura
chr3R	9794186	9794187	CG8516	19.4	30.8	25.1	chr3R_9794187_CG8516
chr4	478956	478957	Asator	15.1	20	17.55	chr4_478957_Asator
chr4	532906	532907	zfh2	20	19.7	19.85	chr4_532907_zfh2
chr4	92946	92947	pan	22.5	20.8	21.65	chr4_92947_pan
chrX	10309093	10309094	alpha-Man-I	24.5	29	26.75	chrX_10309094_alpha-Man-I
chrX	**12331302**	**12331303**	**Ten-a**	**34.8**	**34**	**34.4**	**chrX_12331303_Ten-a**
chrX	16075472	16075473	Tob	23.68	29.32	26.5	chrX_16075473_Tob
chrX	16075887	16075888	Tob	22.2	22	22.1	chrX_16075888_Tob
chrX	16075888	16075889	Tob	21.6	24	22.8	chrX_16075889_Tob
chrX	**16076959**	**16076960**	**Tob**	**20**	**23.3**	**21.65**	**chrX_16076960_Tob**
chrX	16077193	16077194	Tob	17.85	19.15	18.5	chrX_16077194_Tob
chrX	16089317	16089318	Tob	15.2	16.1	15.65	chrX_16089318_Tob
chrX	**3321068**	**3321069**	**dnc**	**22.7**	**28.9**	**25.8**	**chrX_3321069_dnc**
chrX	**3342369**	**3342370**	**dnc**	**17.4**	**22.2**	**19.8**	**chrX_3342370_dnc**
chrX	**6325433**	**6325434**	**CG15894**	**32**	**20.8**	**26.4**	**chrX_6325434_CG15894**
chrX	**9172798**	**9172799**	**mei-P26**	**17.3**	**23.1**	**20.2**	**chrX_9172799_mei-P26**
chrX	9179452	9179453	mei-P26	17.35	22.23	19.79	chrX_9179453_mei-P26
chrX	9188891	9188892	mei-P26	15.8	18.4	17.1	chrX_9188892_mei-P26

774
775

BIBLIOGRAPHY:

Alberti S, Gladfelter A, Mittag T (2019) Considerations and Challenges in Studying Liquid-Liquid Phase Separation and Biomolecular Condensates. *Cell* 176: 419-434

Alberti S, Mateju D, Mediani L, Carra S (2017) Granulostasis: Protein Quality Control of RNP Granules. *Frontiers in Molecular Neuroscience* 10

Andrusiak MG, Sharifnia P, Lyu X, Wang Z, Dickey AM, Wu Z, Chisholm AD, Jin Y (2019) Inhibition of Axon Regeneration by Liquid-like TIAR-2 Granules. *Neuron* 104: 290-304.e298

Ash PEA, Lei S, Shattuck J, Boudeau S, Carlomagno Y, Medalla M, Mashimo BL, Socorro G, Al-Mohanna LFA, Jiang L *et al* (2021) TIA1 potentiates tau phase separation and promotes generation of toxic oligomeric tau. *Proceedings of the National Academy of Sciences* 118: e2014188118

Azkanaz M, Rodríguez López A, De Boer B, Huiting W, Angrand P-O, Vellenga E, Kampinga HH, Bergink S, Martens JH, Schuringa JJ *et al* (2019) Protein quality control in the nucleolus safeguards recovery of epigenetic regulators after heat shock. *eLife* 8

Babinchak WM, Surewicz WK (2020) Liquid–Liquid Phase Separation and Its Mechanistic Role in Pathological Protein Aggregation. *Journal of Molecular Biology* 432: 1910-1925

Bah A, Forman-Kay JD (2016) Modulation of Intrinsically Disordered Protein Function by Post-translational Modifications. *Journal of Biological Chemistry* 291: 6696-6705

Bah A, Vernon RM, Siddiqui Z, Krzeminski M, Muhandiram R, Zhao C, Sonenberg N, Kay LE, Forman-Kay JD (2015) Folding of an intrinsically disordered protein by phosphorylation as a regulatory switch. *Nature* 519: 106-109

Bakthavachalu B, Huelsmeier J, Sudhakaran IP, Hillebrand J, Singh A, Petrauskas A, Thiagarajan D, Sankaranarayanan M, Mizoue L, Anderson EN *et al* (2018) RNP-Granule Assembly via Ataxin-2 Disordered Domains Is Required for Long-Term Memory and Neurodegeneration. *Neuron* 98: 754-766.e754

Becker LA, Huang B, Bieri G, Ma R, Knowles DA, Jafar-Nejad P, Messing J, Kim HJ, Soriano A, Auburger G *et al* (2017) Therapeutic reduction of ataxin-2 extends lifespan and reduces pathology in TDP-43 mice. *Nature* 544: 367-371

Berlow RB, Dyson HJ, Wright PE (2015) Functional advantages of dynamic protein disorder. *FEBS Lett* 589: 2433-2440

Bevilacqua PC, Williams AM, Chou H-L, Assmann SM (2022) RNA multimerization as an organizing force for liquid–liquid phase separation. *RNA* 28: 16-26

Biogen, 2021. https://clinicaltrials.gov/ct2/show/NCT04494256.

Boeynaems S, Dorone Y, Marian A, Shabardina V, Huang G, Kim G, Sanyal A, Şen N-E, Docampo R, Ruiz-Trillo I *et al* (2021) Poly(A)-binding protein is an ataxin-2 chaperone that emulsifies biomolecular condensates. *bioRxiv*: 2021.2008.2023.457426

Brandmann T, Fakim H, Padamsi Z, Youn JY, Gingras AC, Fabian MR, Jinek M (2018) Molecular architecture of LSM14 interactions involved in the assembly of mRNA silencing complexes. *Embo j* 37

Buchan JR (2014) mRNP granules. *RNA Biology* 11: 1019-1030

Calabretta S, Richard S (2015) Emerging Roles of Disordered Sequences in RNA-Binding Proteins. *Trends Biochem Sci* 40: 662-672

Cao X, Jin X, Liu B (2020) The involvement of stress granules in aging and aging-associated diseases. *Aging Cell* 19

Chou A, Krukowski K, Jopson T, Zhu PJ, Costa-Mattioli M, Walter P, Rosi S (2017) Inhibition of the integrated stress response reverses cognitive deficits after traumatic brain injury. *Proc Natl Acad Sci U S A* 114: E6420-e6426

Cirulli ET, Lasseigne BN, Petrovski S, Sapp PC, Dion PA, Leblond CS, Couthouis J, Lu YF, Wang Q, Krueger BJ *et al* (2015) Exome sequencing in amyotrophic lateral sclerosis identifies risk genes and pathways. *Science* 347: 1436-1441

Couthouis J, Hart MP, Erion R, King OD, Diaz Z, Nakaya T, Ibrahim F, Kim H-J, Mojsilovic-Petrovic J, Panossian S *et al* (2012) Evaluating the role of the FUS/TLS-related gene EWSR1 in amyotrophic lateral sclerosis. *Human Molecular Genetics* 21: 2899-2911

Damrath E, Heck MV, Gispert S, Azizov M, Nowock J, Seifried C, Rüb U, Walter M, Auburger G (2012) ATXN2-CAG42 Sequesters PABPC1 into Insolubility and Induces FBXW8 in Cerebellum of Old Ataxic Knock-In Mice. *PLoS Genetics* 8: e1002920

De Graeve F, Besse F (2018) Neuronal RNP granules: from physiological to pathological assemblies. *Biological Chemistry* 399: 623-635

Decker CJ, Teixeira D, Parker R (2007) Edc3p and a glutamine/asparagine-rich domain of Lsm4p function in processing body assembly in Saccharomyces cerevisiae. *J Cell Biol* 179: 437-449

Deo RC, Bonanno JB, Sonenberg N, Burley SK (1999) Recognition of Polyadenylate RNA by the Poly(A)-Binding Protein. *Cell* 98: 835-845

Elden AC, Kim HJ, Hart MP, Chen-Plotkin AS, Johnson BS, Fang X, Armakola M, Geser F, Greene R, Lu MM *et al* (2010) Ataxin-2 intermediate-length polyglutamine expansions are associated with increased risk for ALS. *Nature* 466: 1069-1075

Formicola N, Vijayakumar J, Besse F (2019) Neuronal ribonucleoprotein granules: Dynamic sensors of localized signals. *Traffic* 20: 639-649

Gilks N, Kedersha N, Ayodele M, Shen L, Stoecklin G, Dember LM, Anderson P (2004) Stress granule assembly is mediated by prion-like aggregation of TIA-1. *Mol Biol Cell* 15: 5383-5398

874 Ginsberg SD, Galvin JE, Chiu TS, Lee VM, Masliah E, Trojanowski JQ (1998) RNA
875 sequestration to pathological lesions of neurodegenerative diseases. *Acta Neuropathol* 96: 487-
876 494
877
878 Gomes E, Shorter J (2019) The molecular language of membraneless organelles. *J Biol Chem*
879 294: 7115-7127
880
881 Hachet O, Ephrussi A (2004) Splicing of oskar RNA in the nucleus is coupled to its cytoplasmic
882 localization. *Nature* 428: 959-963
883
884 Halliday M, Radford H, Zents KAM, Molloy C, Moreno JA, Verity NC, Smith E, Ortori CA,
885 Barrett DA, Bushell M *et al* (2017) Repurposed drugs targeting eIF2α-P-mediated translational
886 repression prevent neurodegeneration in mice. *Brain* 140: 1768-1783
887
888 Han TW, Kato M, Xie S, Wu LC, Mirzaei H, Pei J, Chen M, Xie Y, Allen J, Xiao G *et al*
889 (2012) Cell-free formation of RNA granules: bound RNAs identify features and components
890 of cellular assemblies. *Cell* 149: 768-779
891
892 Harlen KM, Churchman LS (2017) The code and beyond: transcription regulation by the RNA
893 polymerase II carboxy-terminal domain. *Nature Reviews Molecular Cell Biology* 18: 263-273
894
895 Hetz C, Zhang K, Kaufman RJ (2020) Mechanisms, regulation and functions of the unfolded
896 protein response. *Nature Reviews Molecular Cell Biology* 21: 421-438
897
898 Hochberg-Laufer H, Schwed-Gross A, Neugebauer KM, Shav-Tal Y (2019) Uncoupling of
899 nucleo-cytoplasmic RNA export and localization during stress. *Nucleic Acids Research* 47:
900 4778-4797
901
902 Hofweber M, Dormann D (2019) Friend or foe—Post-translational modifications as regulators
903 of phase separation and RNP granule dynamics. *Journal of Biological Chemistry* 294: 7137-
904 7150
905
906 Huelsmeier J, Walker E, Bakthavachalu B, Ramaswami M (2021) A C-terminal ataxin-2
907 disordered region promotes Huntingtin protein aggregation and neurodegeneration in
908 Drosophila models of Huntington's disease. *G3 (Bethesda)* 11
909
910 Hyman AA, Weber CA, Jülicher F (2014) Liquid-Liquid Phase Separation in Biology. *Annual*
911 *Review of Cell and Developmental Biology* 30: 39-58
912
913 Inagaki H, Hosoda N, Tsuiji H, Hoshino S-I (2020) Direct evidence that Ataxin-2 is a
914 translational activator mediating cytoplasmic polyadenylation. *Journal of Biological*
915 *Chemistry* 295: 15810-15825
916
917 Ivanov P, Kedersha N, Anderson P (2019) Stress Granules and Processing Bodies in
918 Translational Control. *Cold Spring Harb Perspect Biol* 11
919
920 Jain A, Vale RD (2017) RNA phase transitions in repeat expansion disorders. *Nature* 546: 243-
921 247
922

Järvelin AI, Noerenberg M, Davis I, Castello A (2016) The new (dis)order in RNA regulation. *Cell Commun Signal* 14: 9

Jiang S, Fagman JB, Chen C, Alberti S, Liu B (2020) Protein phase separation and its role in tumorigenesis. *eLife* 9

Jiménez-López D, Guzmán P (2014) Insights into the evolution and domain structure of ataxin-2 proteins across eukaryotes. *BMC Research Notes* 7: 453

Kaehler C, Isensee J, Nonhoff U, Terrey M, Hucho T, Lehrach H, Krobitsch S (2012) Ataxin-2-like is a regulator of stress granules and processing bodies. *PLoS One* 7: e50134

Kato M, Han TW, Xie S, Shi K, Du X, Wu LC, Mirzaei H, Goldsmith EJ, Longgood J, Pei J *et al* (2012) Cell-free formation of RNA granules: low complexity sequence domains form dynamic fibers within hydrogels. *Cell* 149: 753-767

Kedersha N, Anderson P (2007) Mammalian stress granules and processing bodies. *Methods Enzymol* 431: 61-81

Kedersha N, Panas MD, Achorn CA, Lyons S, Tisdale S, Hickman T, Thomas M, Lieberman J, McInerney GM, Ivanov P *et al* (2016) G3BP-Caprin1-USP10 complexes mediate stress granule condensation and associate with 40S subunits. *J Cell Biol* 212: 845-860

Kedersha NL, Gupta M, Li W, Miller I, Anderson P (1999) RNA-Binding Proteins Tia-1 and Tiar Link the Phosphorylation of Eif-2α to the Assembly of Mammalian Stress Granules. *Journal of Cell Biology* 147: 1431-1442

Khong A, Parker R (2020) The landscape of eukaryotic mRNPs. *RNA* 26: 229-239

Kiebler MA, Bassell GJ (2006) Neuronal RNA granules: movers and makers. *Neuron* 51: 685-690

Kim G, Gautier O, Tassoni-Tsuchida E, Ma XR, Gitler AD (2020) ALS Genetics: Gains, Losses, and Implications for Future Therapies. *Neuron* 108: 822-842

Kim H-J, Raphael AR, Ladow ES, Mcgurk L, Weber RA, Trojanowski JQ, Lee VM-Y, Finkbeiner S, Gitler AD, Bonini NM (2014) Therapeutic modulation of eIF2α phosphorylation rescues TDP-43 toxicity in amyotrophic lateral sclerosis disease models. *Nature Genetics* 46: 152-160

Kim HJ, Kim NC, Wang YD, Scarborough EA, Moore J, Diaz Z, MacLea KS, Freibaum B, Li S, Molliex A *et al* (2013) Mutations in prion-like domains in hnRNPA2B1 and hnRNPA1 cause multisystem proteinopathy and ALS. *Nature* 495: 467-473

Kim TH, Payliss BJ, Nosella ML, Lee ITW, Toyama Y, Forman-Kay JD, Kay LE (2021) Interaction hot spots for phase separation revealed by NMR studies of a CAPRIN1 condensed phase. *Proc Natl Acad Sci U S A* 118

Knowles RB, Sabry JH, Martone ME, Deerinck TJ, Ellisman MH, Bassell GJ, Kosik KS (1996) Translocation of RNA Granules in Living Neurons. *The Journal of Neuroscience* 16: 7812

Kozlov G, Safaee N, Rosenauer A, Gehring K (2010) Structural basis of binding of P-body-associated proteins GW182 and ataxin-2 by the Mlle domain of poly(A)-binding protein. *J Biol Chem* 285: 13599-13606

Kwon I, Kato M, Xiang S, Wu L, Theodoropoulos P, Mirzaei H, Han T, Xie S, Corden Jeffry L, McKnight Steven L (2013) Phosphorylation-Regulated Binding of RNA Polymerase II to Fibrous Polymers of Low-Complexity Domains. *Cell* 155: 1049-1060

Latonen L (2019) Phase-to-Phase With Nucleoli – Stress Responses, Protein Aggregation and Novel Roles of RNA. *Frontiers in Cellular Neuroscience* 13: 151

Lee J, Yoo E, Lee H, Park K, Hur JH, Lim C (2017) LSM12 and ME31B/DDX6 Define Distinct Modes of Posttranscriptional Regulation by ATAXIN-2 Protein Complex in Drosophila Circadian Pacemaker Neurons. *Mol Cell* 66: 129-140.e127

Lee KH, Zhang P, Kim HJ, Mitrea DM, Sarkar M, Freibaum BD, Cika J, Coughlin M, Messing J, Molliex A *et al* (2016) C9orf72 Dipeptide Repeats Impair the Assembly, Dynamics, and Function of Membrane-Less Organelles. *Cell* 167: 774-788.e717

Li YR, King OD, Shorter J, Gitler AD (2013) Stress granules as crucibles of ALS pathogenesis. *J Cell Biol* 201: 361-372

Lim C, Allada R (2013) ATAXIN-2 activates PERIOD translation to sustain circadian rhythms in Drosophila. *Science* 340: 875-879

Lin Y, Currie SL, Rosen MK (2017) Intrinsically disordered sequences enable modulation of protein phase separation through distributed tyrosine motifs. *J Biol Chem* 292: 19110-19120

Lin Y, Protter SW, David, Rosen K, Michael, Parker R (2015) Formation and Maturation of Phase-Separated Liquid Droplets by RNA-Binding Proteins. *Molecular Cell* 60: 208-219

Liu EY, Cali CP, Lee EB (2017) RNA metabolism in neurodegenerative disease. *Dis Model Mech* 10: 509-518

Machida K, Shigeta T, Yamamoto Y, Ito T, Svitkin Y, Sonenberg N, Imataka H (2018) Dynamic interaction of poly(A)-binding protein with the ribosome. *Scientific Reports* 8: 17435
Mallucci GR, Klenerman D, Rubinsztein DC (2020) Developing Therapies for Neurodegenerative Disorders: Insights from Protein Aggregation and Cellular Stress Responses. *Annual Review of Cell and Developmental Biology* 36: 165-189

Mandrioli J, Mediani L, Alberti S, Carra S (2020) ALS and FTD: Where RNA metabolism meets protein quality control. *Semin Cell Dev Biol* 99: 183-192

Mangus DA, Evans MC, Jacobson A (2003) Poly(A)-binding proteins: multifunctional scaffolds for the post-transcriptional control of gene expression. *Genome Biol* 4: 223

Maniatis T, Reed R (2002) An extensive network of coupling among gene expression machines. *Nature* 416: 499-506

Martin KC, Ephrussi A (2009) mRNA localization: gene expression in the spatial dimension. *Cell* 136: 719-730

Matheny T, Van Treeck B, Huynh TN, Parker R (2021) RNA partitioning into stress granules is based on the summation of multiple interactions. *RNA* 27: 174-189

McCann C, Holohan EE, Das S, Dervan A, Larkin A, Lee JA, Rodrigues V, Parker R, Ramaswami M (2011) The Ataxin-2 protein is required for microRNA function and synapse-specific long-term olfactory habituation. *Proc Natl Acad Sci U S A* 108: E655-662

McMahon AC, Rahman R, Jin H, Shen JL, Fieldsend A, Luo W, Rosbash M (2016) TRIBE: Hijacking an RNA-Editing Enzyme to Identify Cell-Specific Targets of RNA-Binding Proteins. *Cell* 165: 742-753

Murray DT, Kato M, Lin Y, Thurber KR, Hung I, McKnight SL, Tycko R (2017) Structure of FUS Protein Fibrils and Its Relevance to Self-Assembly and Phase Separation of Low-Complexity Domains. *Cell* 171: 615-627.e616

Murthy AC, Dignon GL, Kan Y, Zerze GH, Parekh SH, Mittal J, Fawzi NL (2019) Molecular interactions underlying liquid−liquid phase separation of the FUS low-complexity domain. *Nature Structural & Molecular Biology* 26: 637-648

Nonhoff U, Ralser M, Welzel F, Piccini I, Balzereit D, Yaspo ML, Lehrach H, Krobitsch S (2007) Ataxin-2 interacts with the DEAD/H-box RNA helicase DDX6 and interferes with P-bodies and stress granules. *Mol Biol Cell* 18: 1385-1396

Patel A, Lee HO, Jawerth L, Maharana S, Jahnel M, Hein MY, Stoynov S, Mahamid J, Saha S, Franzmann TM *et al* (2015) A Liquid-to-Solid Phase Transition of the ALS Protein FUS Accelerated by Disease Mutation. *Cell* 162: 1066-1077

Preissler S, Ron D (2019) Early Events in the Endoplasmic Reticulum Unfolded Protein Response. *Cold Spring Harb Perspect Biol* 11

Protter DSW, Parker R (2016) Principles and Properties of Stress Granules. *Trends Cell Biol* 26: 668-679

Protter DSW, Rao BS, Van Treeck B, Lin Y, Mizoue L, Rosen MK, Parker R (2018) Intrinsically Disordered Regions Can Contribute Promiscuous Interactions to RNP Granule Assembly. *Cell Rep* 22: 1401-1412

Ramaswami M, Taylor JP, Parker R (2013) Altered ribostasis: RNA-protein granules in degenerative disorders. *Cell* 154: 727-736

Rayman JB, Karl KA, Kandel ER (2018) TIA-1 Self-Multimerization, Phase Separation, and Recruitment into Stress Granules Are Dynamically Regulated by Zn2+. *Cell Reports* 22: 59-71

Saito M, Hess D, Eglinger J, Fritsch AW, Kreysing M, Weinert BT, Choudhary C, Matthias P (2019) Acetylation of intrinsically disordered regions regulates phase separation. *Nat Chem Biol* 15: 51-61

Satterfield TF, Pallanck LJ (2006) Ataxin-2 and its Drosophila homolog, ATX2, physically assemble with polyribosomes. *Hum Mol Genet* 15: 2523-2532

Schuller AP, Wojtynek M, Mankus D, Tatli M, Kronenberg-Tenga R, Regmi SG, Dip PV, Lytton-Jean AKR, Brignole EJ, Dasso M *et al* (2021) The cellular environment shapes the nuclear pore complex architecture. *Nature* 598: 667-671

Scoles DR, Meera P, Schneider MD, Paul S, Dansithong W, Figueroa KP, Hung G, Rigo F, Bennett CF, Otis TS *et al* (2017) Antisense oligonucleotide therapy for spinocerebellar ataxia type 2. *Nature* 544: 362-366

Shin Y, Brangwynne CP (2017) Liquid phase condensation in cell physiology and disease. *Science* 357

Shulman JM, Feany MB (2003) Genetic Modifiers of Tauopathy in Drosophila. *Genetics* 165: 1233-1242

Sidrauski C, Mcgeachy AM, Ingolia NT, Walter P (2015) The small molecule ISRIB reverses the effects of eIF2α phosphorylation on translation and stress granule assembly. *eLife* 4

Singh A, Hulsmeier J, Kandi AR, Pothapragada SS, Hillebrand J, Petrauskas A, Agrawal K, Rt K, Thiagarajan D, Jayaprakashappa D *et al* (2021) Antagonistic roles for Ataxin-2 structured and disordered domains in RNP condensation. *eLife* 10

Strome S, Wood WB (1982) Immunofluorescence visualization of germ-line-specific cytoplasmic granules in embryos, larvae, and adults of Caenorhabditis elegans. *Proc Natl Acad Sci U S A* 79: 1558-1562

Sudhakaran IP, Hillebrand J, Dervan A, Das S, Holohan EE, Hülsmeier J, Sarov M, Parker R, VijayRaghavan K, Ramaswami M (2014) FMRP and Ataxin-2 function together in long-term olfactory habituation and neuronal translational control. *Proc Natl Acad Sci U S A* 111: E99-E108

Taylor JP, Brown RH, Cleveland DW (2016) Decoding ALS: from genes to mechanism. *Nature* 539: 197-206

Tillotson R, Selfridge J, Koerner MV, Gadalla KKE, Guy J, De Sousa D, Hector RD, Cobb SR, Bird A (2017) Radically truncated MeCP2 rescues Rett syndrome-like neurological defects. *Nature* 550: 398-401

Toretsky JA, Wright PE (2014) Assemblages: functional units formed by cellular phase separation. *J Cell Biol* 206: 579-588

Trapnell C, Pachter L, Salzberg SL (2009) TopHat: discovering splice junctions with RNA-Seq. *Bioinformatics* 25: 1105-1111

Van Treeck B, Parker R (2018) Emerging Roles for Intermolecular RNA-RNA Interactions in RNP Assemblies. *Cell* 174: 791-802

Van Treeck B, Protter DSW, Matheny T, Khong A, Link CD, Parker R (2018) RNA self-assembly contributes to stress granule formation and defining the stress granule transcriptome. *Proc Natl Acad Sci U S A* 115: 2734-2739

Vogler TO, Wheeler JR, Nguyen ED, Hughes MP, Britson KA, Lester E, Rao B, Betta ND, Whitney ON, Ewachiw TE *et al* (2018) TDP-43 and RNA form amyloid-like myo-granules in regenerating muscle. *Nature* 563: 508-513

Wang F, Li J, Fan S, Jin Z, Huang C (2020) Targeting stress granules: A novel therapeutic strategy for human diseases. *Pharmacological Research* 161: 105143

Wheeler JR, Matheny T, Jain S, Abrisch R, Parker R (2016) Distinct stages in stress granule assembly and disassembly. *eLife* 5

Wolozin B, Ivanov P (2019) Stress granules and neurodegeneration. *Nature Reviews Neuroscience* 20: 649-666

Wong YL, Lebon L, Edalji R, Lim HB, Sun C, Sidrauski C (2018) The small molecule ISRIB rescues the stability and activity of Vanishing White Matter Disease eIF2B mutant complexes. *eLife* 7

Xie J, Kozlov G, Gehring K (2014) The "tale" of poly(A) binding protein: the MLLE domain and PAM2-containing proteins. *Biochim Biophys Acta* 1839: 1062-1068

Yang P, Mathieu C, Kolaitis RM, Zhang P, Messing J, Yurtsever U, Yang Z, Wu J, Li Y, Pan Q *et al* (2020) G3BP1 Is a Tunable Switch that Triggers Phase Separation to Assemble Stress Granules. *Cell* 181: 325-345.e328

Yi H, Park J, Ha M, Lim J, Chang H, Kim VN (2018) PABP Cooperates with the CCR4-NOT Complex to Promote mRNA Deadenylation and Block Precocious Decay. *Mol Cell* 70: 1081-1088.e1085

Yokoshi M, Li Q, Yamamoto M, Okada H, Suzuki Y, Kawahara Y (2014) Direct binding of Ataxin-2 to distinct elements in 3' UTRs promotes mRNA stability and protein expression. *Mol Cell* 55: 186-198

Yoshida M, Yoshida K, Kozlov G, Lim NS, De Crescenzo G, Pang Z, Berlanga JJ, Kahvejian A, Gehring K, Wing SS *et al* (2006) Poly(A) binding protein (PABP) homeostasis is mediated by the stability of its inhibitor, Paip2. *The EMBO Journal* 25: 1934-1944

Youn JY, Dyakov BJA, Zhang J, Knight JDR, Vernon RM, Forman-Kay JD, Gingras AC (2019) Properties of Stress Granule and P-Body Proteomes. *Mol Cell* 76: 286-294

Zhang K, Daigle JG, Cunningham KM, Coyne AN, Ruan K, Grima JC, Bowen KE, Wadhwa H, Yang P, Rigo F *et al* (2018) Stress Granule Assembly Disrupts Nucleocytoplasmic Transport. *Cell* 173: 958-971.e917

Zhang Y, Ling J, Yuan C, Dubruille R, Emery P (2013) A role for Drosophila ATX2 in activation of PER translation and circadian behavior. *Science* 340: 879-882

1173 Zyryanova AF, Kashiwagi K, Rato C, Harding HP, Crespillo-Casado A, Perera LA, Sakamoto
1174 A, Nishimoto M, Yonemochi M, Shirouzu M *et al* (2021) ISRIB Blunts the Integrated Stress
1175 Response by Allosterically Antagonising the Inhibitory Effect of Phosphorylated eIF2 on
1176 eIF2B. *Mol Cell* 81: 88-103.e106
1177